

The role of Taper Ratio on the Energy Harvesting Capabilities of Inverted Flags

A report submitted to The University of Manchester for the degree of
Aerospace Engineering
in the Faculty of Science and Engineering

Kieran Currie-Cathey ID:10834350

Supervised by Dr. Mostafa A. Nabawy

Contents

List of Figures	v
List of Tables	vi
Nomenclature	vii
Abstract	viii
Declaration	ix
Copyright	ix
Ackowledgements	x
1 Introduction	1
1.1 Motivation	1
1.2 Aims	2
1.3 Objectives	2
2 Literature Review	2
2.1 Introduction	2
2.2 Types of Flags and How They Work	2
2.3 The Physics of Flags	3
2.4 Non-Dimensional Governing Parameters	3
2.5 Morphological and Planform Effects	7
2.6 Summary	8
3 Methodology and Experimental Design	10
3.1 Flag Design	10
3.2 Flag Manufacturing	11
3.3 Clamp Design and Fabrication	12
3.4 Experimental Setup and Procedure	13
4 Post Processing and Theory	16
4.1 Tracking	16
4.2 Post Processing Theory	17
4.2.1 Angular Amplitude	17
4.2.2 Frequency	17
5 Results and Discussion	18
5.1 Mass Ratio Verification	19
5.2 Taper Ratio Investigation	20
5.3 Fluid Energy	23
6 Conclusions, Limitations, and Further Work	25

6.1	Conclusion	25
6.2	Research Question	25
6.3	Limitations and Future Work	26
6.3.1	Materials Used and Manufacturing	26
6.3.2	Energy Harvesting	26
7	Appendix A: Initial Project Plan and Proposal	30
7.1	Project Proposal	30
7.2	Methodology	30
7.2.1	Proposed Experiments	30
7.2.2	Experimental Design	31
7.2.3	Performance Metrics	31
8	Project Planning	31
8.1	Semester 1	31
8.1.1	WP1 - Literature Review	32
8.1.2	WP2 - Hands-on Learning and Research	32
8.1.3	WP3 - Project Proposal	32
8.1.4	WP4 - Design and Fabrication	32
8.1.5	Semester 1 Gantt Chart	32
8.2	Semester 2	33
8.2.1	WP5 - Testing	33
8.2.2	WP6 - Work on Deliverables	33
8.2.3	Semester 2 Gantt Chart	34
9	Critical Reflection	34
9.1	Table of Risks	34
9.2	Not Enough Lab Access/Time	35
9.3	Flags Break	35
9.4	Broken Equipment	35
9.5	Time Management	35
9.6	Not Enough Materials	36
10	Conclusions and Future Work	36
11	Semester 2 Gantt Chart and Project Reflection	36
11.1	Project Management Reflection	38
12	Appendix B: MATLAB Post-Processing	38
12.1	Frequency and Amplitude Calculation Function	38
12.2	Fluid Energy Calculations	39
12.3	Mass Ratio Plotting and Bending Stiffness Calculations	39
12.4	Taper Ratio Plotting and Bending Stiffness Calculations	42
12.5	Example Processing Script: $\lambda = 2.353$	47

13 Appendix C: Example Data Sets for $\lambda = 2.353$	50
13.1 12.44 ms ⁻¹ Raw Data	50
13.2 Processing script output data	56

List of Figures

1	Application of Remote Energy Harvesting (<i>Irrigation Scheduling Using Soil Water Tension Sensors - Alabama Cooperative Extension System</i> n.d.)	1
2	Comparing a regular and inverted flag setup, showing the differences in orientation and configuration relative to the oncoming flow (Yang, Nabawy, et al. 2021)	3
3	Three typical behaviours of inverted flags in superimposed view of the flag with (a) straight (b) limit cycle flapping and (c) full deflection. Image produced in Tang, N. S. Liu, and Lu 2015.	3
4	Schematic of inverted flag with the leading edge free and the trailing edge clamped. The dashed straight line is the initial position of the flag. A is the vertical distance between the flag displacement, and s is the curvilinear coordinate from the fixed end (Kim et al. 2013).	4
5	Fully deflected flag, exhibiting a similar behaviour to that of a traditional flag, with low amplitude flapping not suitable for energy harvesting. Produced in Tang, N. S. Liu, and Lu 2015, representative of any flag in the $\beta = 0.1$ and below range.	5
6	Peak-to-peak amplitude A/L vs β . (a) High mass ratio $O(1)$ $H/L = 1.3$ (\square); $H/L = 1.1$ (\circ); $H/L = 1.0$ (\triangle). (b) Low mass ratio $O(10^{-3})$ $H/L = 2.0$ (\square); $H/L = 1.6$ (\circ); $H/L = 1.3$ (\triangle) (Kim et al. 2013).	6
7	Summary of flag performance. Plots of aspect ratio and speed (increasing and decreasing) vs (a) amplitude, and (b) frequency (Yang, Nabawy, et al. 2021).	7
8	Results obtained both numerically (a) and experimentally (b) by Ojo et al. 2019a. Similar results were obtained in other mentioned studies.	8
9	Inverted flags of constant taper and aspect ratio, with differing thicknesses to quantify the effect of mass ratio.	10
10	All flags designed and manufactured for quantifying the effects of λ on inverted flag dynamics.	11
11	Example of the residual curvature after the flag has been place in a clamp. The thickness here is 0.2 mm and shows the most curvature, but is present in the majority of flags.	12
12	Clamp Design: based on NACA 0018 aerofoil bisected along chord line. Two halves were manufactured and the flag was sandwiched between the two halves.	13
13	Combined flag and clamp structure.	13
14	Test section of the wind tunnel with camera mounted above.	14
15	Furness Controls Portable Calibrator and Precision Manometer (FCO560)	15
16	Side view of experimental setup with final clamp used and example flag.	15
17	Schematic of final tapered flag experimental setup.	16
18	The initial setup of a video in Physlets Tracker (left) and the final setup (right) after tracking has taken place. These images are taken from videos recording the 0.05 mm thickness mass ratio test flag.	16

19	Visualisation of the code theory in Section 12. Quadrants 1 and 2 directly work out the angle to the y - axis (deflection from resting state). Quadrants 3 and 4 work out the angles between the flag and the x - axis. This requires adding 90° to the values before doubling.	17
20	Example data output after tracking, for the same flag and video as mentioned in Figure 18. This data is for the partial deflection flapping regime. The transition between limit cycle flapping and full deflection.	18
21	Example of Physlets tracker calculated sine curve and associated A B C D values.	18
22	Mass ratio behaviour verification flags. Plotting Wind speed [ms^{-1}] against Frequency [Hz] and Amplitude [°]	19
23	Taper ratio test flags. Plotting Wind speed [ms^{-1}] against Frequency [Hz] and Amplitude [°]	21
24	Taper ratio test flags. Plotting A/L vs β for increasing and decreasing wind speeds.	22
25	Fluid energy imparted onto the surface of the flag to reach the maximum flapping amplitude at a given windspeed.	24
26	Theoretical bending energy generated in each flag at maximum deflection for a given wind speed.	24
27	Gantt chart in the initial project proposal, red cells signify due dates.	30
28	Semester 1 Gantt Chart and Planning. Red cells signify due dates.	33
29	Semester 2 Gantt Chart and Planning. Red cells signify due dates. Other course deadlines are left out as they are not available yet.	34
30	Revised semester 2 Gantt Chart and Planning. Red cells signify due dates. Other course deadlines are left out.	36

List of Tables

1	Papers reviewed (15): all are either referenced in the literature review, or have been read for background knowledge and research.	9
2	Flags designed for the purpose of verifying the effects of changing mass ratio on inverted tapered flags.	10
3	Flags designed for the purpose of verifying the effects of changing λ on inverted tapered flags.	11
4	Dynamics characteristics of each tapered flag for overall measurements. U_{Stop} is the wind speed at which the flag transitioned from limit cycle flapping to rest.	20
5	Risks to current project plan.	34
6	12.44 ms^{-1} raw data output from Physlets Tracker software	50
7	Wind speed, angular amplitude, frequency and fluid energy calculated outputs	56

Nomenclature

β Dimensionless Bending Stiffness

λ Taper Ratio

μ Mass Ratio

ν Poisson's Ratio

ρ Density

θ Angular Amplitude

[]_f Pertaining to Fluid

[]_r Pertaining to Flag Root

[]_s Pertaining to Solid/Sheet

[]_t Pertaining to Flag Tip

AR Aspect Ratio

B Flexural Rigidity

C Chord

E Young's Modulus

h Flag Thickness

L Flag Length

S Flag Area

U Flow Velocity

Abstract

Finding sources of renewable energy is essential to maintaining the stability of the environment. Battery usage is globally at an all time high, and if methods can be found to replace these in small scale portable electronics such as remote sensors, then they should be explored. In recent years, inverted flags have grown in popularity within research into sources of renewable energy. By attaching piezoelectric materials to their surface, energy can be extracted when the flag oscillates under an oncoming flow. The behaviour of rectangular flags, and the effect of AR , has been studied relatively extensively with their dynamics well documented. However, little research into the effects of changing other geometrical parameters has been studied. The objective of this paper is to study how tapering the inverted flags changes their dynamics. This work presents an initial look into the effects of taper on inverted flags, including flapping frequency and angular amplitude, as well as relative deformation compared to the length of the flag (to remain consistent with previous research). To do this, differing flags were designed to first verify if the observed dynamics in rectangular flags are also present in tapered. Then flags of differing taper were tested to ascertain the general effect of changing taper. Flag behaviour was recorded at differing wind speeds to give displacement and time data, which was then translated into flapping frequencies and angular amplitude. The results show that behaviour is relatively similar to rectangular flags, with some key differences. Frequencies vary significantly across differing values of λ , however angular amplitude is relatively consistent across the set. Whilst the frequencies are promising, the increase is not so substantial that harvesting more energy is possible. As such, more research is required to verify this.

Declaration

No portion of the work referred to in the dissertation has been submitted in support of an application for another degree or qualification of this or any other university or other institute of learning.

Copyright

- i) The author of this dissertation (including any appendices and/or schedules to this dissertation) owns certain copyright or related rights in it (the “Copyright”) and s/he has given The University of Manchester certain rights to use such Copyright, including for administrative purposes.
- ii) Copies of this dissertation, either in full or in extracts and whether in hard or electronic copy, may be made only in accordance with the Copyright, Designs and Patents Act 1988 (as amended) and regulations issued under it or, where appropriate, in accordance with licensing agreements which the University has entered into. This page must form part of any such copies made.
- iii) The ownership of certain Copyright, patents, designs, trademarks and other intellectual property (the “Intellectual Property”) and any reproductions of copyright works in the dissertation, for example graphs and tables (“Reproductions”), which may be described in this dissertation, may not be owned by the author and may be owned by third parties. Such Intellectual Property and Reproductions cannot and must not be made available for use without the prior written permission of the owner(s) of the relevant Intellectual Property and/or Reproductions.
- iv) Further information on the conditions under which disclosure, publication and commercialisation of this dissertation, the Copyright and any Intellectual Property and/or Reproductions described in it may take place is available in the University IP Policy, in any relevant Dissertation restriction declarations deposited in the University Library, and The University Library’s regulations.

Acknowledgements

I would like to thank my project supervisor Dr. Mostafa Nabawy for his continued support and time throughout the project. Working with Dr. Nabawy has pushed me to work harder and explore topics I had not considered before. I would also like to thank Akshat Naik for his time, dedication, and support throughout this project, whom without reaching the end would not have been possible.

Thanks also to Babar Khan, whilst we did not have the same project the area of study was similar, and it is always welcome and refreshing to have someone to bring a new perspective to the research.

I would also like to thank my close friends and family for the advice, help, and love they have all provided me with. Words cannot do justice to how much I value them.

1 Introduction

1.1 Motivation

Within the last several decades there has been a significant increase in demand for renewable energy. The continuous burning of fossil fuels such as coal, gas, oil etc. has had, and will continue to have, detrimental effects on our environment. Many studies have been conducted on the effect of rising carbon emissions, concluding that global temperatures will rise leading to droughts, mass flooding, an increase in tropical storms, mass migration, food shortages and many more harmful consequences (“The Carbon Cycle” 2011, “GLOBAL CLIMATE” 2022, Hansen et al. 2013).

As a result, there has been a significant rise in the demand for renewable energy from sources such as wind, solar, water flows and geothermal for the use of powering houses, buildings, essentially any everyday energy consumer. A new and emerging market however is ambient energy harvesting for powering remote sensors and small-scale portable electronics to be used in a variety of applications such as environmental and process monitoring, smart city applications and resource management ((Kerr and Ostrovsky 2003), (Turner et al. 2003), (Sishodia, Ray, and Singh 2020)).



Figure 1: Application of Remote Energy Harvesting (*Irrigation Scheduling Using Soil Water Tension Sensors - Alabama Cooperative Extension System n.d.*)

Remote sensors are normally not very power intensive, usually requiring power levels in the range of micro-Watt to milli-Watt. Whilst such sensors can be deployed with conventional batteries, these pose several issues such as limited operational time thus requiring frequent replacement, and being safely disposed of, often containing harmful chemicals that add to the current environmental issues. Consistently replacing the battery supply of a large network of sensors would also prove challenging and expensive. Ambient energy conversion is therefore a useful and impact area of research.

Ambient wind energy harvesting using piezoelectric materials is a more recent area of interest, with much study going into the flapping dynamics of flags (Yu, Y. Liu, and Amandoese 2019, Sader, Huertas-Cerdeira, and Gharib 2016, Kim et al. 2013). General study has found that the conventional flag type (fixed leading edge, free trailing edge) is not a particularly effective method for ambient energy harvesting due to its requirements of high wind speeds to induce large amplitude flapping, however the inverted flag (fixed trailing edge, free leading edge) is an area of research with proof of concepts on their ability to harvest wind energy ((Silva-Leon et al. 2019), (Yang, Nabawy, et al. 2021)).

1.2 Aims

This individual project is concerned with the effect of taper ratio on the flapping dynamics of inverted flags, particularly on the critical wind speeds for flapping regime transition, and whether it is worth the investment of constructing said flags in a custom manner as opposed to with off the shelf components.

1.3 Objectives

1. Perform a comprehensive review of previous literature and research on inverted flags.
2. Conduct experiments where mass ratio varies, whilst aspect ratio and taper ratio are kept constant.
3. Conduct experiments where aspect ratio is constant, whilst mass ratio and taper ratio varies.
4. Discuss the effects of taper ratio on inverted flag behaviour, and if the effects of mass ratio are consistent with previous literature.

2 Literature Review

2.1 Introduction

Whilst the area of study on inverted flags is a relatively new area of research, extensive study has been conducted in some aspects of their behaviour when subjected to oncoming flows. In order to progress knowledge on their behaviour, it is critical that we first review the research that has already been done, and use it to guide the direction of our subsequent research. First, the type of flag that will be studied here will be described and compared to a standard flag to highlight the differences in their behaviour. From there the governing parameters of the flapping regime will be described and discussed as well as the effects of plan form changes and the limited knowledge on morphological effects.

2.2 Types of Flags and How They Work

For the purpose of this study there will be two types of flags, the inverted and the standard flag. The standard flag is the one most people are familiar with, i.e. a fixed leading edge and a free trailing edge. The earliest study found in this literature review with regards to the dynamics of a standard flag was the works of Taneda 1968 (Waving Motions of Flags). In this study it is concluded that the instability in the flag occurs due to the interaction of the flags inertial and elastic forces, with the induced fluid forces. As the standard flag begins to move in a flow, the changing shape relative to the oncoming flow increases the aerodynamic loads upon it. This drives the flag to increase its displacement until a balance is reached between the driving forces, and high amplitude flapping occurs. For the standard flag to experience the high amplitude flapping regime it requires a large driving fluid force, in other words, a high wind speed, often much higher than everyday winds can reach, as such a bluff body is often placed upstream to induce oscillation of the downstream fluid structure (Kim et al. 2013).

The form of an inverted flag is essentially the opposite to a standard flag, the trailing edge is fixed to a clamp of some form, whilst the leading edge faces into the oncoming flow and is free to vibrate about the fixed trailing edge. They also are normally constructed out of different materials, such as very thin

sheets of metal. One of the advantages of an inverted flag is that they are easily unstable at low critical flow velocities, and depending on design, can have high excitation amplitude. The dynamics of inverted flags were first studied by Kim et al. 2013. They found that the formation of leading and trailing edge vortices from the slight deformation of the flag change the forces on the flags surface leading to larger amplitude flapping, assuming that the restoring elastic force of the flag is not dominant. A comparison of a traditional and inverted flag setup is shown in Figure 2.

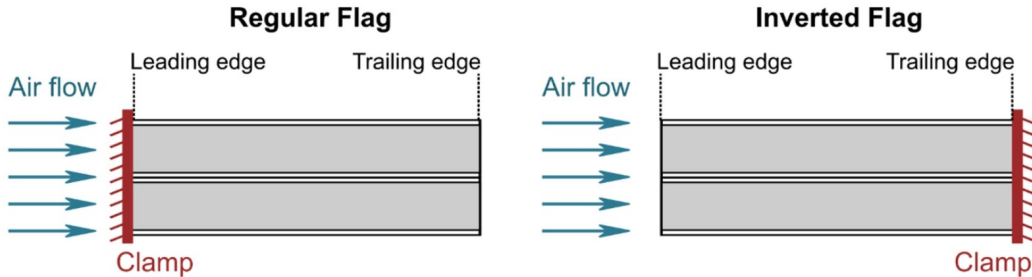


Figure 2: Comparing a regular and inverted flag setup, showing the differences in orientation and configuration relative to the oncoming flow (Yang, Nabawy, et al. 2021)

2.3 The Physics of Flags

The behaviour of the inverted flag in a flow can be described in three general regimes; straight mode, limit cycle flapping mode, and fully deflected (Kim et al. 2013), shown in Figure 3. Inverted flags oscillate due to one of two reasons, induced flapping via vortices in the flow creating pressure differences over the surface of the flag, or self induced via fluid-elastic instability. Vortex induced flapping is predominantly exclusive to heavy flags, for the flags considered in this literature review, and the rest of the study, the motion is due to the imbalance of fluid pressure forces and internal elastic restoring forces.

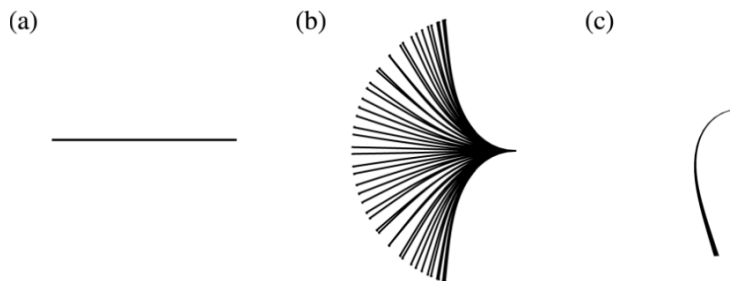


Figure 3: Three typical behaviours of inverted flags in superimposed view of the flag with (a) straight (b) limit cycle flapping and (c) full deflection. Image produced in Tang, N. S. Liu, and Lu 2015.

2.4 Non-Dimensional Governing Parameters

There are two main dimensionless parameters that are widely used to categorise the motion of inverted flags, the bending stiffness β (essentially a dimensionless flow speed), and the mass ratio (ratio of flag mass to fluid force) μ :

$$\beta = \frac{B}{\rho_f U^2 L^3} \quad (1)$$

Where B is the flexural rigidity as defined in Equation 2, ρ_f is the fluid density, U is the velocity of the oncoming flow and L is the sheet length in the direction of the flow.

$$B = \frac{Eh^3}{12(1 - \nu^2)} \quad (2)$$

Where E and ν is the Young's modulus and Poisson's ratio respectively, and h is the sheet thickness.

$$\mu = \frac{\rho_s h}{\rho_f L} \quad (3)$$

Where ρ_f and ρ_s and the fluid and sheet density respectively. The bending stiffness can be thought of as the ratio of the flag's bending force to the inertial force the fluid imposes on the flag with a high β denoting a stiff flag, or low flow speed, and a low β denoting the more flexible flag or a high flow speed. Regarding this literature review, the first appearance found of these parameters were in the derivation of governing parameters of standard flag behaviour subject to a free stream velocity conducted by Kornecki, Dowell, and O'Brien 1976. The first major study found in this literature review regarding β for inverted flags was conducted by Kim et al. 2013.

In their paper on the flapping dynamics of inverted flags Kim et al. set out to find the ranges of β which corresponded to each flapping regime. Their experiments were conducted in an open loop wind tunnel. The wind tunnel cross-section 1.2 m x 1.2 m, with free-stream velocity ranging between 2.2 and 8.5 ms⁻¹. The material used was a polycarbonate (Young's Modulus $E = 2.38 \times 10^9$ Nm², Poisson's ratio $\nu = 0.38$, and density $\rho_s = 1.2 \times 10^3$ kgm³) with thickness h of 0.8 mm. The aspect ratio (H/L) ranged from 1.0 to 1.3. The general setup for the experiment is pictured in Figure 4.

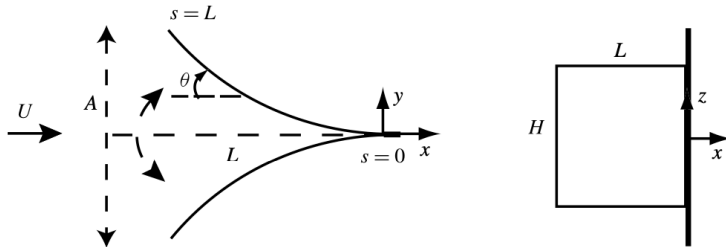


Figure 4: Schematic of inverted flag with the leading edge free and the trailing edge clamped. The dashed straight line is the initial position of the flag. A is the vertical distance between the flag displacement, and s is the curvilinear coordinate from the fixed end (Kim et al. 2013).

They concluded that, relatively regardless of aspect ratio, that inverted flags have specific ranges of β where each regime would occur. For β higher than 0.3, straight mode would occur with slight flutter, but the peak-to-peak amplitude A/L was less than 0.2. Deflection of such a small amount would not produce enough strain energy to effectively convert to electrical energy. For β lower than 0.1 the sheet exhibits the fully deflected mode, i.e. the base bends around the clamp and the sheet largely resembles the configuration as a standard flag with A/L in the same range as that of the straight orientation, shown in Figure 5.

Between these two quasi-static modes ($0.1 < \beta < 0.3$) is where the limit cycle flapping occurs. Periodic deformation was measured with a nearly constant A/L . A/L was found to increase drastically in the flapping mode, reaching a maximum value of between 1.7 and 1.8. For the range of $0.1 < \beta < 0.2$ the



Figure 5: Fully deflected flag, exhibiting a similar behaviour to that of a traditional flag, with low amplitude flapping not suitable for energy harvesting. Produced in Tang, N. S. Liu, and Lu 2015, representative of any flag in the $\beta = 0.1$ and below range.

amplitude of the flapping slightly decreased, the sheet continued to bend past the tips maximum $|y|$ which results in a decrease in the $|y|$ at maximum deformation. Whilst not discussed within the study, at a brief thought this maximum deformation is most likely due to the higher free-stream velocity experienced by the sheet (higher β means either a stiffer sheet or higher wind speeds, as the sheet is not changing it must be due to the higher wind speeds). Whilst the internal elastic restoring force will increase with increased deflection, it is clear that it does not scale proportionally with the increase in aerodynamic loading.

These findings align relatively well with another study conducted by Yu, Y. Liu, and Amandolese 2019 in "A Review on Fluid-Induced Flag Vibrations". They found the same three flapping regimes within their flag, and within similar ranges of β . For $\beta > 0.4$ the flag remained in straight mode, for $0.1 < \beta < 0.4$ large amplitude cycle flapping, and $\beta < 0.1$ full deflection about the fixed trailing edge, with maximum A/L between 1.6 - 1.9. It is worth noting that in the range of $0.3 < \beta < 0.4$ the flapping was found to be asymmetric. Whilst the results are relatively similar between the two separate studies, Kim et al. 2013 conducted an experimental analysis whilst Yu, Y. Liu, and Amandolese 2019 conducted a numerical and computational analysis, which often cannot account for all variables present in physical experiments and is therefore not always enough to thoroughly test designs of any kind.

The other primary governing parameter is the mass ratio μ . Also first seen to be derived in Kornecki, Dowell, and O'Brien 1976, studying the dynamics of standard flags. For standard flags, μ has a much more pronounced effect on the flapping regime experienced than it does on inverted flags. In a paper by Connell and Yue 2007 conducting a study on the dynamics of a flag in the uniform stream, it was found that for standard flags mass ratio was the primary governing parameter of behaviour as opposed to bending stiffness. Using numerical simulations it was found that for $\mu = 0.025$ a steady straight configuration is experienced, for $0.05 < \mu < 0.1$ stable flapping, and $\mu > 0.125$ chaos, i.e. flapping is experienced but the frequency and the amplitudes are non-constant.

The first time that a study on the effects of mass ratio on the inverted flag configuration were investigated was also in Kim et al. 2013 which produced a significantly different relationship between flapping regimes and μ . The same experiments conducted in the wind tunnel were also conducted in water for lower mass ratios (on the order of $O(10^{-3})$ as opposed to $O(1)$ in the wind tunnel). It was found that different orders of mass ratio had very little effect on the behaviour of the flags. For a low mass ratio of $O(10^{-3})$ the flag also flapped with $A/L > 0.2$ in the range of $0.2 < \beta < 0.4$, but that the large amplitude oscillations occurred in a smaller range of $0.2 < \beta < 0.25$. They also noted

that "in many cases of the flapping mode, the sheet does not cross the $y = 0$ line after rebounding, but continues to bend and rebound on one side" (Kim et al. 2013), for that reason A/L is decreased compared to that of high mass ratios.

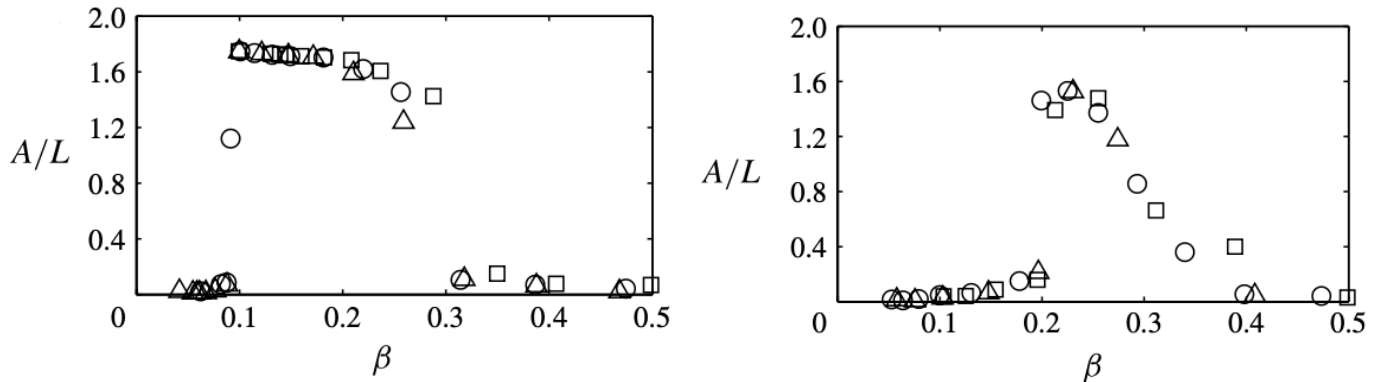


Figure 6: Peak-to-peak amplitude A/L vs β . (a) High mass ratio $O(1)$ $H/L = 1.3$ (\square); $H/L = 1.1$ (\circ); $H/L = 1.0$ (\triangle). (b) Low mass ratio $O(10^{-3})$ $H/L = 2.0$ (\square); $H/L = 1.6$ (\circ); $H/L = 1.3$ (\triangle) (Kim et al. 2013).

Comparing the graphs in Figure 6, we can also see that an effect of the changing the order of mass ratio is the result in a steeper transition from straight to limit cycle flapping mode to full deflection for higher orders of mass ratio. This agrees with the works of Yu, Y. Liu, and Amandolese 2019. It is unclear however, as to why Kim et al. 2013 used flags of different aspect ratios in their investigation of low mass ratio compared to high mass ratio, it could simply be down to the water tunnel having a smaller cross-section, but it still begs the question as to what the results would look like if they had used the same flags for both studies. Regardless, comparing the graphs above it would be reasonable to conclude that whilst mass ratio is a governing parameter, the effect of it's order is minor.

Recently, Yang, Nabawy, et al. 2021 conducted more in depth study onto the effect of mass ratio (and other factors) on flapping regimes. A sample of 12 flags were studied, with 3 different mass ratios, and 3 different aspect ratios per mass ratio (the aspect ratio effects will be discussed in Section 2.5). The mass ratios studied were $\mu = 7, 9.2$ and 14 . It was found that for increasing mass ratios of the same order (in comparison to the difference in orders studied by Kim et al. 2013) that larger mass ratios require a higher velocity oncoming flow to transition from the straight regime to the limit cycle flapping and subsequently the fully deflected mode. Similarly the same is true for the reverse transitions, i.e. the velocity of the oncoming flow is at a higher value for the transition from fully deflected, to flapping, to straight mode.

As well as this, it was also found that an increase in μ also leads to an increase in the effective working speeds. The mass ratio of 7 had an average working range of 1.53 ms^{-1} , whereas for the mass ratio of 14 had an average working range of 5.23 ms^{-1} . It is worth noting that within these mass ratios there are very different aspect ratios. Each of which has it's own effect on the flags dynamics, but the effect of mass ratio on the working range still stands. Flapping amplitude and frequency also dramatically increases with increasing mass ratio. Figure 7 summarises the combined findings of the effects of μ and aspect ratio.

Between these two studies on the effect of mass ratio on the behaviour of inverted flags we can deduce that the order of the mass ratio is unlikely to change the behaviour when subject to a flow (Kim et al.

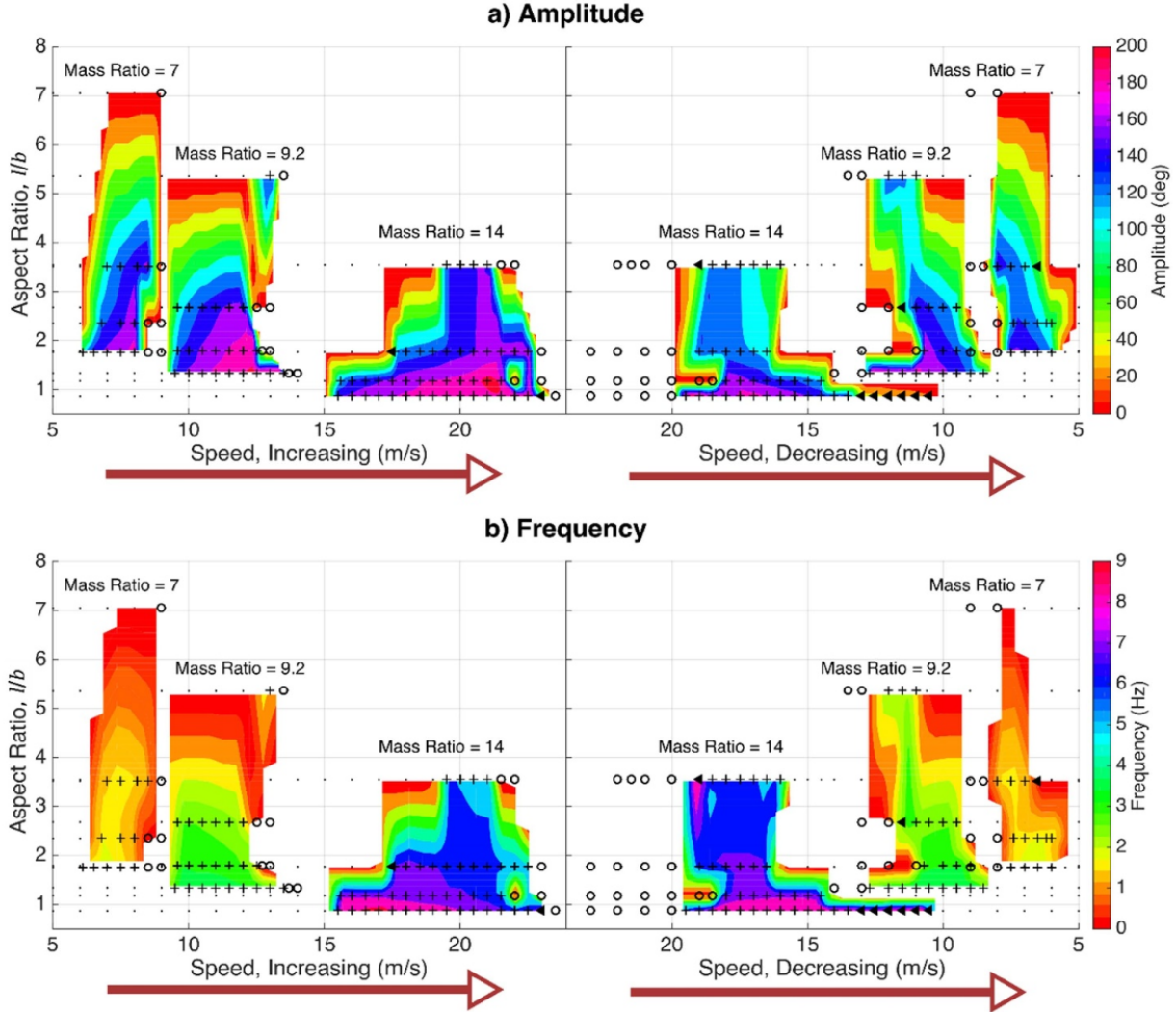


Figure 7: Summary of flag performance. Plots of aspect ratio and speed (increasing and decreasing) vs (a) amplitude, and (b) frequency (Yang, Nabawy, et al. 2021).

2013). However, changes to the mass ratio within a certain order, like those studied in Yang, Nabawy, et al. 2021, have a large impact on the flapping frequency, amplitude, and the range of effective wind speeds for the limit cycle flapping. It is worth noting however, that the flags studied in Kim et al. 2013 and Yang, Nabawy, et al. 2021 were not of the same type. Those studied in Kim et al. 2013 were of a single sheet of polycarbonate, whilst those studied in Yang, Nabawy, et al. 2021 were of a composite of PVDF elements sandwiching an elastic layer made of stainless steel. There is much debate as to how to calculate the bending stiffness of composite flags, so it is unclear how this will have affected the results obtained, regardless, it is still likely that the effects of mass ratio will be similar or the same for inverted flags made of just the elastic layer.

2.5 Morphological and Planform Effects

The largest area of study in planform and morphological effects has been on the influence of aspect ratio on flag behaviour (Kim et al. 2013, Yang, Nabawy, et al. 2021, Fan et al. 2019, Ojo et al. 2019a). Between Kim et al. 2013, Ojo et al. 2019a, and Yang, Nabawy, et al. 2021, several different aspect ratios were studied, all producing similar conclusions between the three. The largest range of aspect ratios studied is in Yang, Nabawy, et al. 2021 ranging from 1.76 to 7.05 (these are the aspect ratios of the lowest value of μ ($\mu = 7$) in the study, so as to neglect any effects of mass ratio between this

comparison as much as is possible). Ojo et al. 2019a studied aspect ratios of 1, 2, and 4, whilst Kim et al. 2013 studied aspect ratios of 1.0 to 1.3, all at similar mass ratios.

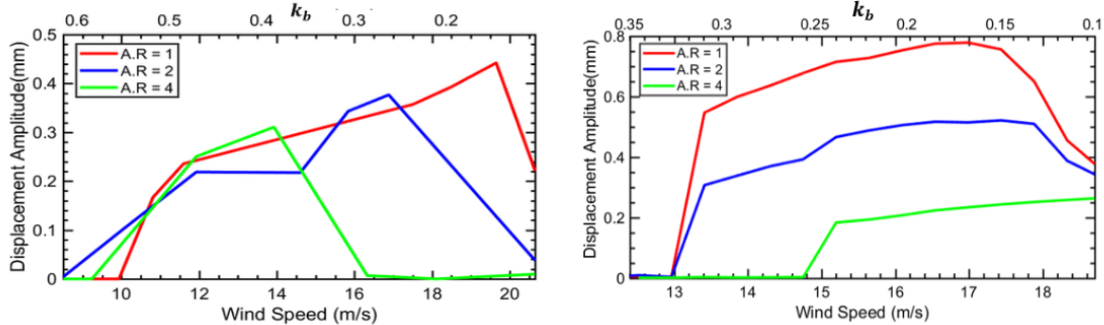


Figure 8: Results obtained both numerically (a) and experimentally (b) by Ojo et al. 2019a. Similar results were obtained in other mentioned studies.

Each paper came to the same conclusions, that for a given mass ratio, the average flapping amplitude and frequency increases with decreasing aspect ratio (shown in Figure 8). The reason for growth in amplitude is related to the projected area, a lower aspect ratio means a wider flag, i.e. H is bigger. This means that a wider flag experiences more fluid pressure force, a higher destabilising force, thus forcing a higher flapping amplitude. The increase in flapping frequency is due to the flags being more massive. This increase in mass leads to a more intense competition between the external fluid pressure force, and the internal elastic restoring forces.

2.6 Summary

To summarise, the primary governing parameters defining the flapping regimes of an inverted flag are bending stiffness β , and mass ratio μ . For β , within the range of effective bending stiffness, as β increases, the amplitude of the flag decreases, assuming all other variables remain constant, this will be due to a decrease in wind speed, leading to a decrease in fluid pressure force. Regarding mass ratio, as μ increases the wind speed to start the onset of high amplitude flapping increases due to the flag being more massive, however, with increasing μ the width of effective wind speeds also increases. Little investigation has been conducted into the effect of the order mass ratio, but from the analysis in Kim et al. 2013, it is a reasonable assumption to say that the order of mass ratio has little effect. More study is required but that is outside the scope of this project.

The main planform effect that has been studied is the effect of changing aspect ratio on the behaviour of the flag. For a given μ , as aspect ratio decreases, the average flapping amplitude and frequency increases. This can be attributed to the area of the flag facing the oncoming flow, and the increase in mass.

No study at the time of this submission has been found regarding the effects of taper ratio on inverted flags. As such, this paper aims to establish the general changes in performance for different taper ratios, and critically discuss whether the extra investment into custom built materials is worth the cost and effort.

Table 1: Papers reviewed (15): all are either referenced in the literature review, or have been read for background knowledge and research.

Papers Reviewed		
Title	Author & Date	Experimental or Computational
Flapping Dynamics of an Inverted Flag	Kim et al. 2013	Experimental
Flapping Dynamics of a Flag in a Uniform Stream	Connell and Yue 2007	Computational
One The Aeroelastic Instability of Two Dimensional Panels in Uniform Incompressible Flow	Kornecki, Dowell, and O'Brien 1976	Experimental & Computational
A Review on Fluid-Induced Flag Vibrations	Yu, Y. Liu, and Amandolese 2019.	Computational
Stability of Slender Inverted Flags and Rods in Uniform Steady Flow	Sader, Huertas-Cerdeira, and Gharib 2016	Experimental & Computational
Large Amplitude flapping of an Inverted Elastic Foil in Uniform Flow with Spanwise Periodicity	Gurugubelli and Jaiman 2019	Experimental & Computational
Effect of Morphology on the Large-Amplitude Flapping Dynamics of an Inverted Flag in a Uniform Flow	Fan et al. 2019	Experimental
Aspect Ratio Effects in Wind Energy Harvesting Using Inverted Piezoelectric Flags	Ojo et al. 2019b	Experimental
Dynamics of Inverted Flags: Experiments and Comparison with Theory	Tavallaeinejad, Salinas, et al. 2021	Experimental & Computational
Planform Geometry Effects of Piezoelectric Wind Energy Harvesting Composite Inverted Flags	Yang, Nabawy, et al. 2021	Experimental
Aspect Ratio Effects in Wind Energy Harvesting Using Piezoelectric Inverted Flags	Ojo et al. 2019a	Experimental & Computational
Large-Amplitude Flapping of an Inverted Flag in a Uniform Steady Flow – a Vortex-Induced Vibration	Sader, Cosse, et al. 2016	Experimental & Computational
Simultaneous Wind and Solar Energy Harvesting with Inverted Flags	Silva-Leon et al. 2019	Experimental
Harvesting Ambient Wind Energy with an Inverted Piezoelectric Flag	Orrego et al. 2017	Experimental
Waving Motions of Flags	Taneda 1968	Experimental
Wing Bending Calculations with a Single set of Equations	Lannoy 2014	Computational
Dynamics of an inverted flexible plate in a uniform flow	Tang, N. S. Liu, and Lu 2015	Computational
Instability and the post-critical behaviour of two-dimensional inverted flags in axial flow	Tavallaeinejad, Païdoussis, et al. 2020	Computational
Wind Energy Harvesting with Vertically Aligned Piezoelectric Inverted Flags	Yang, Cioncolini, et al. 2023	Experimental

3 Methodology and Experimental Design

3.1 Flag Design

Each inverted flag was constructed from a stainless-steel shim by Precision Brand (www.precisionbrand.com; Density: 7900 kg m^{-3} ; Young's Modulus: $Y_e = 193 \text{ GPa}$; Poisson's Ratio: $\nu = 0.25$ (*302 Stainless Steel* n.d.)) which can be found and purchased from RS Components at varying thicknesses (<https://uk.rs-online.com/web/p/steel-shims/0519024>). Whilst the effects of aspect ratio have been studied extensively (see Section 2), the effects of mass ratio remain uncertain. As a result, part of these experiments will be aimed at determining if the effect of mass ratio on flags of rectangular planform is similar/the same for those with tapered planforms. This is also necessary as it is becoming apparent that we are currently unable to separate changing bending stiffness (i.e. EI values, not dimensionless bending stiffness as shown in Equation 1) with changing taper ratio. As such, the effects of mass ratio will first be verified in separate experiments, and then these results can be accounted for when analysing the results of the varying taper experiments. Other equations could be derived to take into account this three dimensionality but this is outside the scope of the project, and additional experiments would be required to verify the integrity of said equations.

Each flag regarding the mass ratio experiments has a taper ratio (λ) = 0.75, with the root and tip chords (C_r , C_t) being 0.1 m and 0.75 m respectively, and a length (L) of 0.13 m. The thickness of the flags were varied across the experiments to vary the mass ratio as shown in Equation 3. A detailed summary of all mass ratio experiment flag properties is shown in Table 2 and Figure 9.

Table 2: Flags designed for the purpose of verifying the effects of changing mass ratio on inverted tapered flags.

Mass Ratio Experiments						
C_r [m]	C_t [m]	L [m]	h [mm]	Area [m^2]	AR [Area/ L^2]	μ
0.1	0.75	0.13	0.05	0.0114	1.486	2.835
0.1	0.75	0.13	0.1	0.0114	1.486	5.669
0.1	0.75	0.13	0.2	0.0114	1.486	11.339

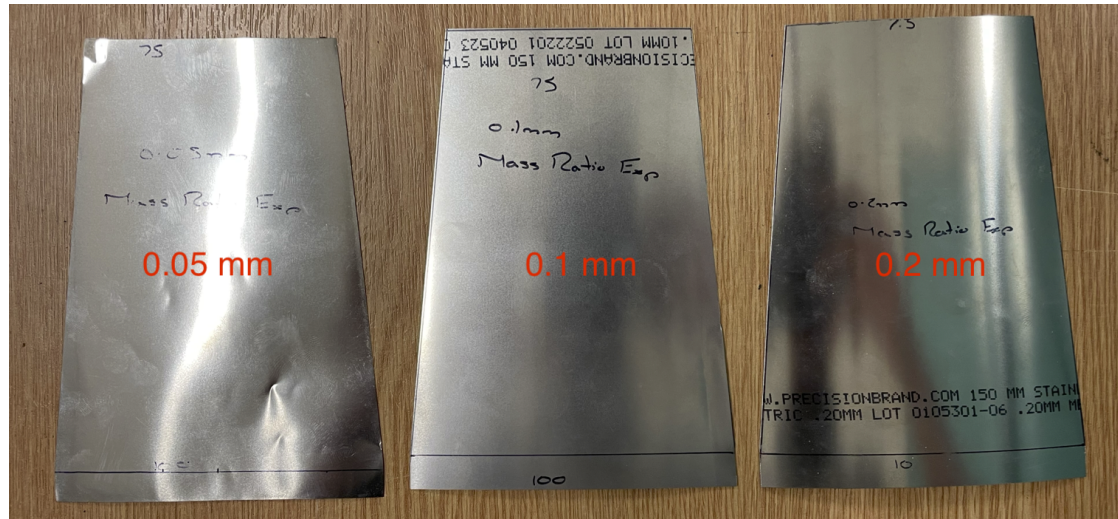


Figure 9: Inverted flags of constant taper and aspect ratio, with differing thicknesses to quantify the effect of mass ratio.

Regarding the flags designed to quantify the effects of taper ratio, each flag had a set AR of 0.75 and

a set h of 0.1 mm. From here, using the formula for the AR , the area of a trapezium (as shown in Equation 4), and defining C_r , C_t can be found, and from there λ can be calculated as well as μ .

$$S = L \cdot \left(\frac{C_r + C_t}{2} \right) \quad (4)$$

In total there are 5 flags of varying λ from $\lambda < 1$ to $\lambda \geq 1$. The majority of the lifting force (i.e. the force causing the flag to bend and oscillate in the flow) is generated at the tip of the flag. Varying λ to sub/sur 1 values allows studying the changes in flapping frequency and amplitude when the lifting force varies along with the elastic restoring force (which is generated at the root, and is a function of the 'amount' of material present). Whilst the changes in λ are non-constant, this is inconsequential as the purpose of this study is to study the general effects of varying λ , as opposed to the finer workings of small, discrete changes in λ . A summary of the flags used to quantify the effects of changing λ is shown in Table 3 and Figure 10.

As previously mentioned, varying λ and μ independently is not possible, as shown by the properties in Table 3. However, μ varies minimally in comparison to λ so it is expected for the changes in behaviour to be dominated by the effects of λ .

Table 3: Flags designed for the purpose of verifying the effects of changing λ on inverted tapered flags.

Taper Ratio Experiments								
No.	C_r [m]	C_t [m]	L [m]	λ	Area [m^2]	AR [Area/ L^2]	μ	C_{Avg} [m]
F1	0.034	0.08	0.076	2.353	0.00433	0.75	8.485	0.057
F2	0.054	0.09	0.096	1.667	0.00691	0.75	6.717	0.072
F3	0.1	0.1	0.1333	1.00	0.0133	0.75	4.837	0.010
F4	0.1	0.078	0.1187	0.78	0.0106	0.75	5.435	0.089
F5	0.08	0.034	0.076	0.425	0.00433	0.75	8.485	0.057

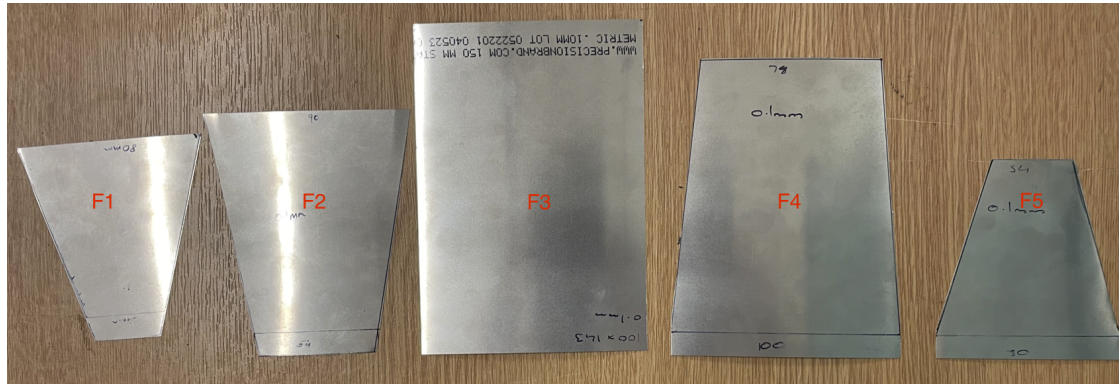


Figure 10: All flags designed and manufactured for quantifying the effects of λ on inverted flag dynamics.

3.2 Flag Manufacturing

For the scope of this project it was not possible to order each flag from either RS Components or Precision Brand independently, this meant that sheets of shim were ordered and manufacturing took place in house. Each sheet arrived rolled for ease of transport, however, this meant that there were residual stresses and deformation present in all of the materials. Slight curvature was present

throughout all of the sheets, which became more exaggerated closer to either end (each sheet came as a 1.25 m × 150 mm roll). Initially heat treatment was considered to flatten the sheets, but concerns over how the thickness of the material would be able to handle the heat and limited material prevented this method. Re-rolling the sheets was also attempted, however this also failed to work. Eventually it was decided to press the sheets under heavy weight for several days to remove the curvature as best as possible. The thinner sheets such (0.05 mm and 0.1 mm) lost some curvature, but the method proved relatively ineffective for the 0.2 mm sheet. The possible effects of said curvature will be discussed in later sections. An example of the residual curvature, demonstrated on the 0.2 mm thickness mass ratio test flag is shown in Figure 11.



Figure 11: Example of the residual curvature after the flag has been place in a clamp. The thickness here is 0.2 mm and shows the most curvature, but is present in the majority of flags.

Regarding fabricating the flags from the sheet material, laser cutting was attempted, but the heat caused deformation along the edges of each flag which we were unable to remove. This meant that each flag would need to be cut by hand. We were able to use a guillotine to ensure that all lines were cut as straight as possible, and each dimension was carefully measured and checked before cutting.

3.3 Clamp Design and Fabrication

Whilst The University of Manchester already has some clamps suitable for this project, research is showing that it may be that the wake created by the flag also has an effect on the behaviour (Yu, Y. Liu, and Amandolese 2019). As a result, we endeavoured to design a new clamp with the aim of producing a more uniform flow in the wake behind the flag. A clamp was designed by bisecting a NACA 0018 aerofoil along the chord line, as shown in Figure 12. The typical trailing edge of the aerofoil would hold the flag (essentially now the leading edge), whilst the typical trailing edge would attach to a rigid pole mounted in the centre of the wind tunnel.

Whilst ideally the aerofoil would not be inverted from it's typical orientation, the thickness of the trailing edge would not allow for the clamp to be mounted inside the wind tunnel. Theoretically, this should produce a more uniform wake, however verification of this is outside the scope of this project, most likely needing some form of PIV testing which is expensive and time consuming. Additionally, there is little mention in previous literature about how the wake development changes performance, and so to be consistent it is of little concern at this stage.

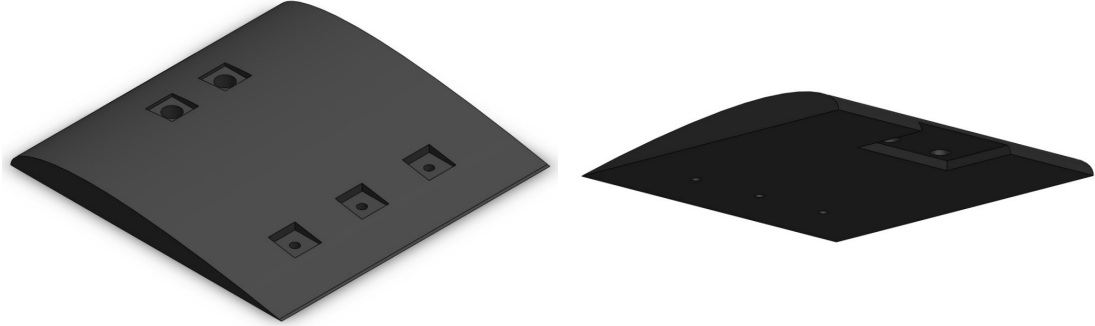


Figure 12: Clamp Design: based on NACA 0018 aerofoil bisected along chord line. Two halves were manufactured and the flag was sandwiched between the two halves.

The clamp itself was resin printed. The three holes near the thin edge are for size M3 screws, the clamping force and friction provided by these screws is what holds the flags in place. The two larger holes are for size M6 screws, these are to attach the clamp to the internal structure of the wind tunnel (descriptions and demonstrations of how will be discussed later on). The clamp is a 0.1 m x 0.1 m square. A combined flag and clamp structure is presented in Figure 13.

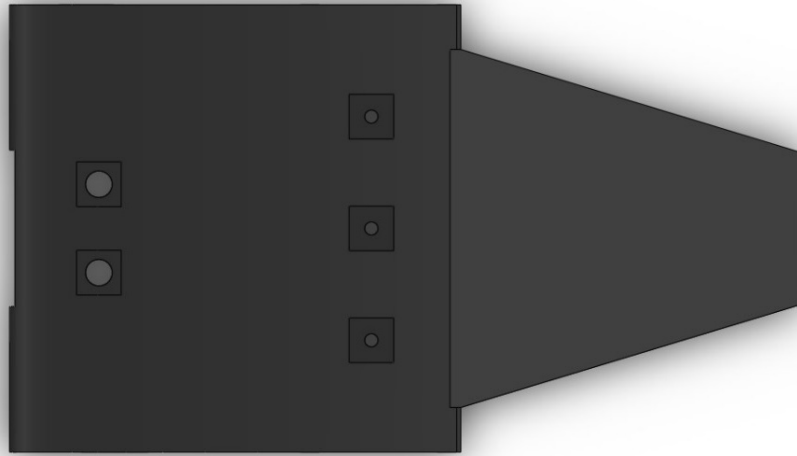


Figure 13: Combined flag and clamp structure.

3.4 Experimental Setup and Procedure

The experimental setup is very similar to that shown in Yang, Nabawy, et al. 2021 as the wind tunnel used is the same (i.e. exactly the same location, control equipment etc.). The clamped edge of the inverted flags were attached to a vertical metal pole located midway through the wind tunnel (Armfield Limited, Ringwood, Uk (www.armfield.co.uk)). The wind tunnel has an octagonal cross-section 350 mm × 350 mm (height x width), Figure 14, capable of reaching air flow velocities from

1.5 to 25 ms⁻¹. Whilst testing the airflow velocity was measured using static/dynamic pressure ports connected to a calibrated pressure manometer (Furness Controls Portable Calibrator and Precision Manometer (FCO560) (www.furness.com/product/fco560/), Figure 15). The motion of the flags was recorded using a digital camera (Nikon D5300 (www.nikonusa.com)), an example video is available at https://youtu.be/_PrE0pt1cxs. The camera was set up with a shutter speed of 1/4000, aperture = F4.2, iso = 1600, resolution 1920 × 1080, and focal length of 29 mm with a capture rate of 60 Hz. The camera was mounted above the test section to capture an overhead view of the flag.

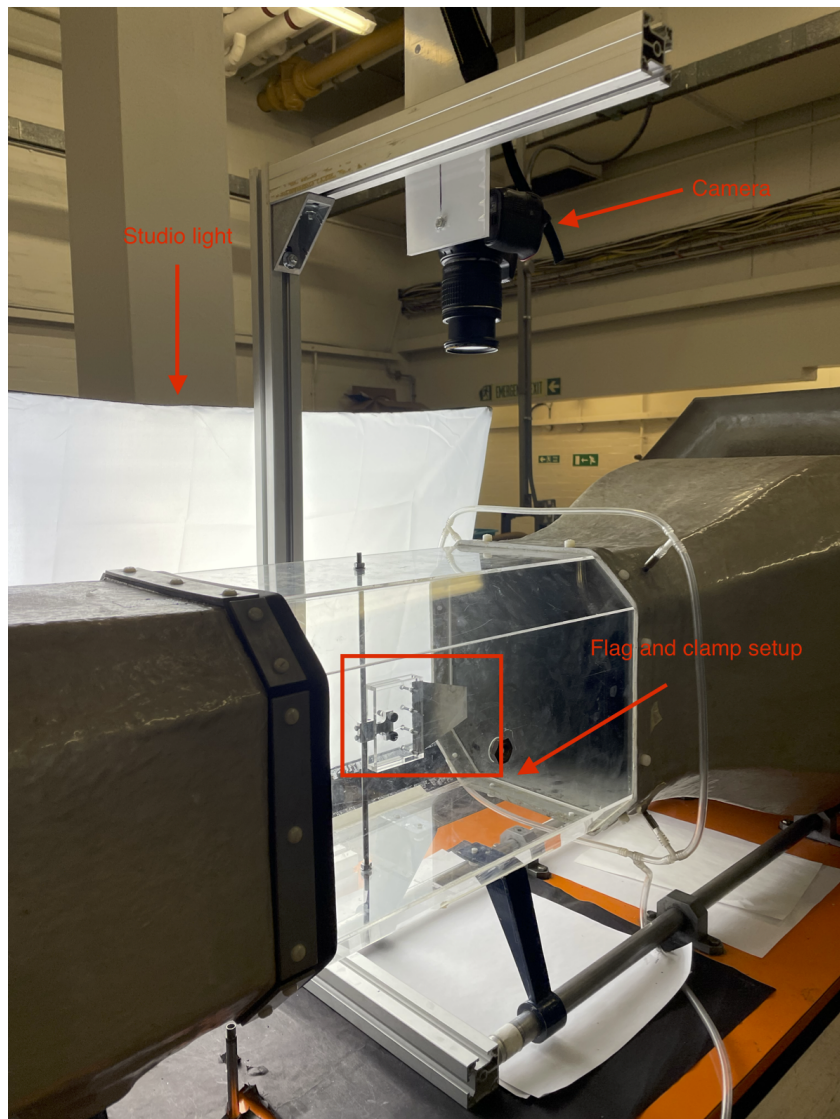


Figure 14: Test section of the wind tunnel with camera mounted above.

A plain white piece of paper was placed below the test section to improve the accuracy of optical tracking. A studio light was also placed next to the test section to improve lighting conditions for the same purpose. The videos were post processed with Tracker version 6.1.6 (<https://phslets.org/tracker/>), a free open-source video analysis modelling tool. The time and displacement data (x , y [mm]) was then exported to MATLAB where a script was written to analyse the displacement to find the frequency and angular amplitude. The motion is characterised by flapping frequency at each recorded wind speed, as well as angular amplitude θ [°], defined as the angle between two flapping extreme positions and where the flag meets the clamp as seen from the top (keeping consistent with previous literature).



Figure 15: Furness Controls Portable Calibrator and Precision Manometer (FCO560)

At the beginning of each test the wind speed was low and the flag aligned with the oncoming flow (to within a couple of degrees - no offset is necessary but it does have effect on the transition flow speeds). The wind speed was gradually increased until the flag began to flap, this wind speed was recorded and a video capture taken. The wind speed was then gradually increased taking videos at different set points until the flag was fully deflected (some flags did not experience this but that will be discussed in Section 5). The wind speed was then gradually reduced until the flag returned to its initial position.

Whilst the clamp designed for this project was suitable for the majority of the flags, for some of the longer flags (i.e. those designed for testing the effects of mass ratio) the tip of the flag extended too close to the end of the transparent test section of the tunnel. This made tracking more challenging and as a result we chose to replace the clamp with one used in Yang, Nabawy, et al. 2021, and to keep consistency between all tests every flag as tested with this different clamp. There is not expected to be minimal difference in the results however, and the trends produced by varying λ will most likely remain unchanged. The setup with the final clamp is presented in Figure 16 and 17.

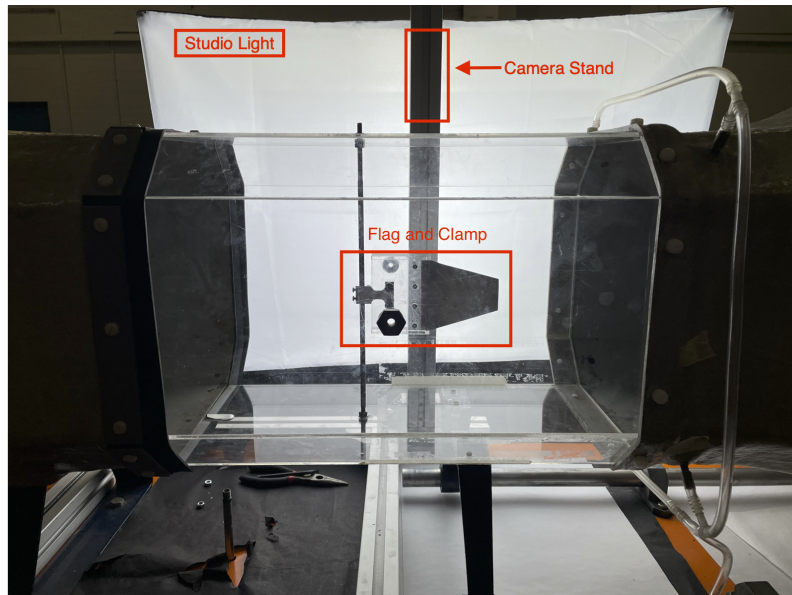


Figure 16: Side view of experimental setup with final clamp used and example flag.

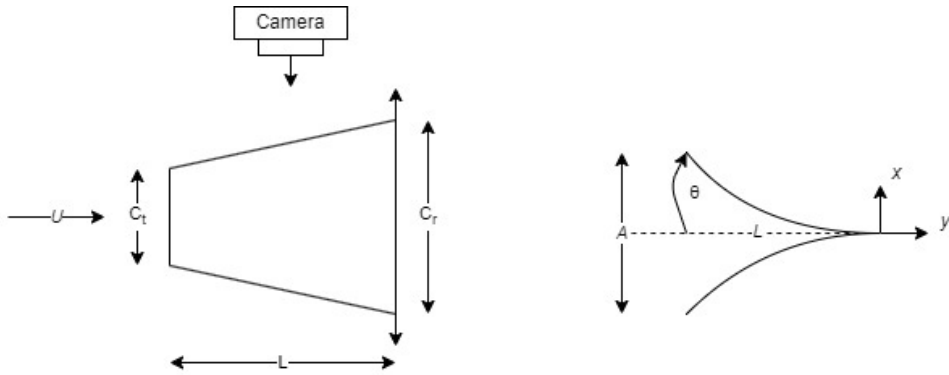


Figure 17: Schematic of final tapered flag experimental setup.

4 Post Processing and Theory

4.1 Tracking

This section details the steps taken and theory behind the post processing so as to remain transparent about how results were obtained and to allow others to remain consistent in research. A full copy of all MATLAB scripts and functions used is presented in Appendix B.

Before being able to process data in MATLAB, first the videos recorded must be converted into useful time and displacement data for analysis. As previously mentioned in Section 3.4 this was done using Physlets Tracker. Each video must be uploaded and each frame tracked. Whilst Tracker has an auto-track function, the changing light over the flag as it moved meant that the auto-track had trouble recognising the tip of the flag in each frame, as such each frame was tracked manually.

Reference geometry must be established as well as an origin. The reference geometry chosen was the thickness of the clamp (19 mm) as this would be constant in every video. Whilst there would be little negative effect, this is small compared to the flapping amplitudes. Ideally a scale would have been imaged in the plan of focus that would also allow calibration of lens distortion. The origin would be placed at the root of the flag/where the flag meets the clamp. The position of the tip of the flag was then recorded in each frame and the software outputs displacement (x, y) and time data. From here the data can be exported as a .txt file and imported into MATLAB. Examples of the tracking software setup and data output are shown in Figures 18 and Appendix C respectively.

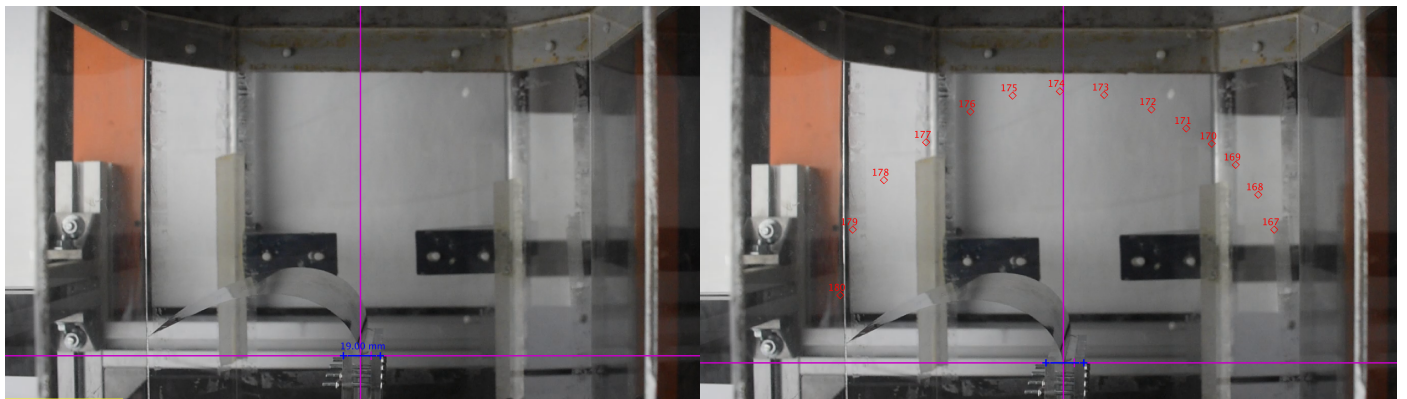


Figure 18: The initial setup of a video in Physlets Tracker (left) and the final setup (right) after tracking has taken place. These images are taken from videos recording the 0.05 mm thickness mass ratio test flag.

4.2 Post Processing Theory

4.2.1 Angular Amplitude

Finding the amplitude is relatively simple compared to the frequency. In the code provided in Appendix B, the x and y data is used to calculate the angle made between either the x or y axis depending on the quadrant, and then doubled. For those quadrants below the x axis, the angles must first be added to 90° , as shown in Figure 19.

From here MATLAB's `findpeaks` function was used to find the maximum angular amplitudes in the data set, which were then averaged. Once every data set had been processed this provided an average θ_{max} for each flag at each tested wind speed.

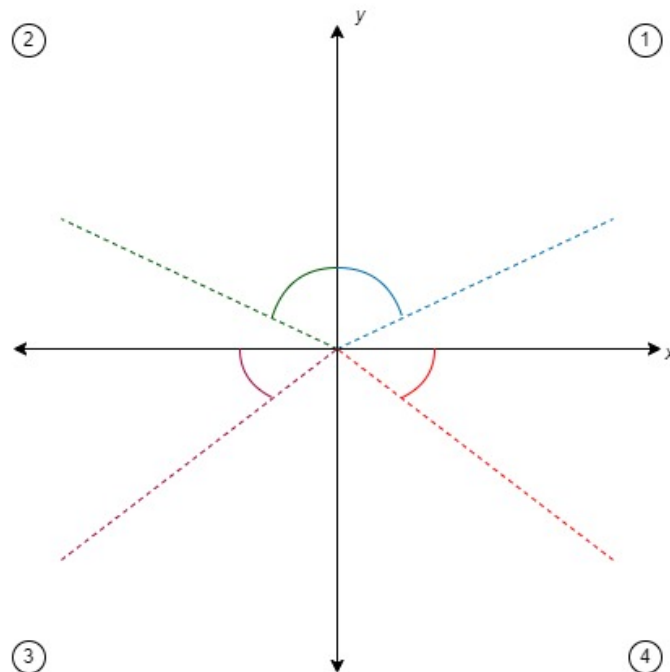


Figure 19: Visualisation of the code theory in Section 12. Quadrants 1 and 2 directly work out the angle to the y -axis (deflection from resting state). Quadrants 3 and 4 work out the angles between the flag and the x -axis. This requires adding 90° to the values before doubling.

4.2.2 Frequency

Calculating frequency is more complex and arguably less accurate because it involves fitting a sine curve to the displacement data. From there the period of the sine curve can be found and converted into a frequency. For some data sets, MATLAB is unable to fit a sine curve due to the nature of the behaviour of the flag. This typically occurs in the chaotic and fully deflected flapping regimes as the behaviour of the flags in these regimes are inconsistent. An example of the displacement-time data for the chaotic regime is shown in Figure 20.

The way to combat this issue is to use the inbuilt Physlets Tracker sine curve fitter to provide values for amplitude [A], angular frequency [B], initial phase [C], and vertical offset [D], which can then be fed into the MATLAB function to plot a sine curve over the data. An example of the Physlets tracker sine curve and associated A B C D values can be seen in Figure 21.

It is worth noting that for these data sets the approximation of frequency is less accurate. This is due to the sine curve being less closely fitted to the actual behaviour of the flag when compared to the

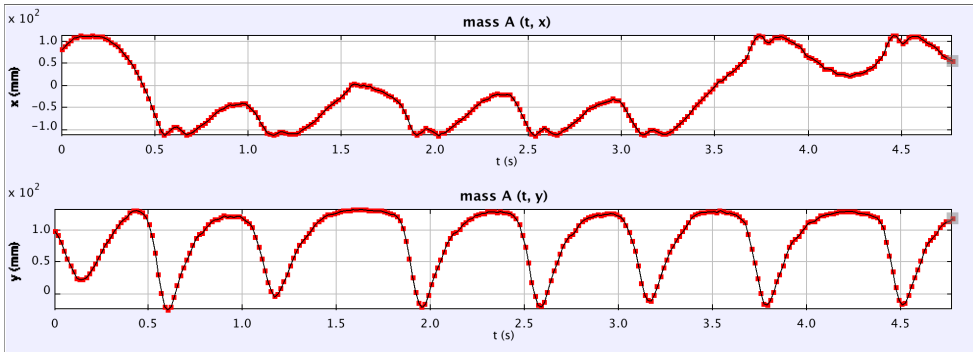


Figure 20: Example data output after tracking, for the same flag and video as mentioned in Figure 18. This data is for the partial deflection flapping regime. The transition between limit cycle flapping and full deflection.

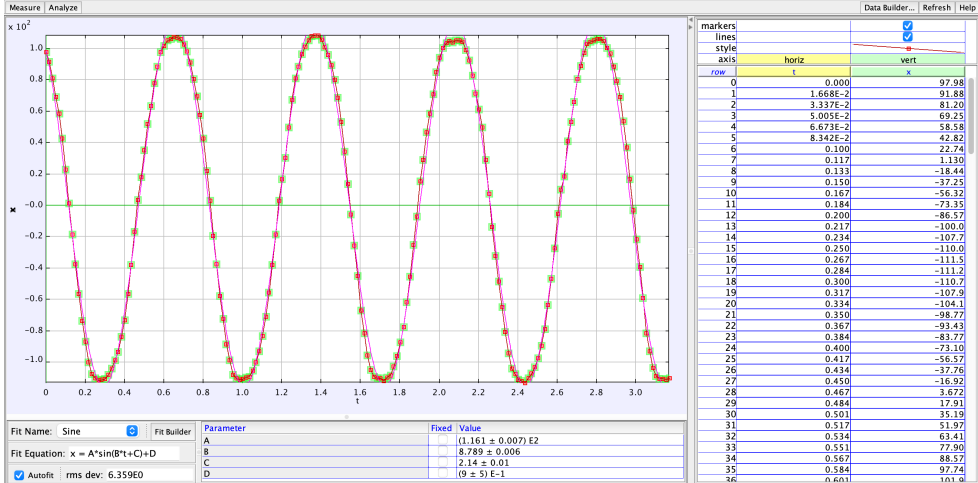


Figure 21: Example of Physlets tracker calculated sine curve and associated A B C D values.

limit cycle flapping modes. However, this is not of significant issue as the area of concern is the limit cycle flapping, and we are more interested in the transition region as opposed to the behaviour after transition.

5 Results and Discussion

In the following subsections the effects of mass ratio are analysed and summarised, before proceeding to a discussion and summary of the effects of taper ratio on the dynamics of inverted flags. The main dynamic states of motion described in Section 2 are clearly observed. At low onset wind velocities, the flag remains in a straight position, sometimes with low amplitude oscillations (it is hard to tell but this could be from general motion of the wind tunnel). Essentially the flag is at rest in equilibrium. As the speed of the oncoming flow increases, there is a certain onset speed (U_{onset}) after which the large amplitude cycle flapping mode occurs. The flag is essentially unstable but the side-to-side motion is relatively symmetrical.

Much of the previous research discussed in Section 2 (such as Kim et al. 2013, Yang, Nabawy, et al. 2021, Silva-Leon et al. 2019) state that there is a specific flow speed at which the flag transitions from limit cycle flapping to full deflection. In these tests this was not strictly observed. Instead there was a small region in which the flag remained predominantly deflected, but at inconsistent time intervals experienced full oscillations momentarily.

The data here is presented in both raw and dimensionless form. The purpose of this study is to characterise how taper ratio effects the performance of inverted flags changes, and it stands that the trends should be present regardless of the format that the data is presented in.

5.1 Mass Ratio Verification

Figure 22 shows the average frequencies and amplitudes of the tested flags with differing mass ratios but constant geometries, as shown in Table 2. Results are displayed for both increasing and decreasing wind speed. Measuring both the increasing and decreasing wind speeds allows for the identification of possible (and present here) hysteresis. As well as, this you can identify possible material memory effects. If present, on the return from full deflection to lower wind speeds, the flag will not be able to return to the oscillation phase it previously experienced.

Looking at Figure 22 it is clear that with increasing μ , the effective working range of wind speeds increases. The higher mass ratio flag (i.e. the thicker flag) having a working range of 4.14 ms^{-1} whilst the lower mass ratio flag has a working range of 1.15 ms^{-1} . Whilst there is no definite consensus between previous works regarding the reason for this, it could be attributed to the higher thickness of the flags. The extra thickness allows for greater resistance to permanent deflection as the wind speed increases, allowing the flag to maintain oscillation for longer. This reason can also be attributed to the higher mass ratio flags requiring higher U_{onset} to transition from equilibrium to oscillation. With greater thickness comes greater opposition to deformation, as such the force provided by the oncoming flow must be higher to allow the flag to start oscillating.

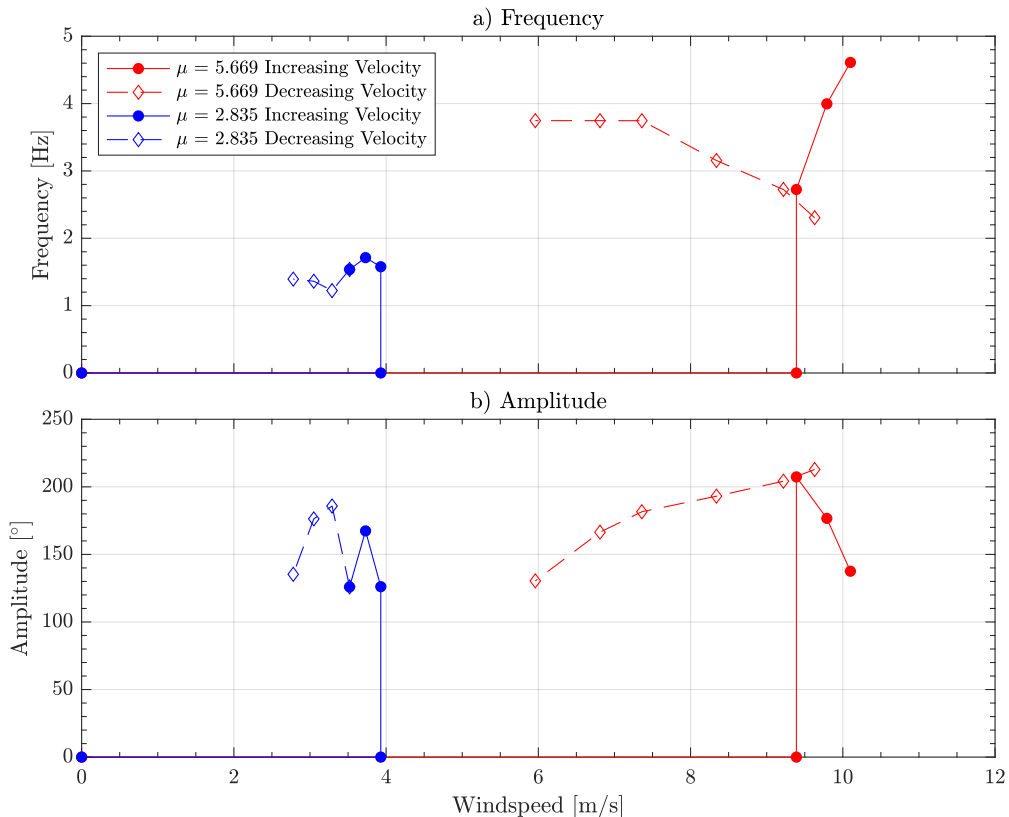


Figure 22: Mass ratio behaviour verification flags. Plotting Wind speed [ms^{-1}] against Frequency [Hz] and Amplitude [$^{\circ}$]

It can also be seen that for the flag to transition from deflection back to oscillation the wind speed has to decrease below the original transition wind speed on the increasing velocity; a phenomenon

attributed to the mechanical properties of the flag (Yang, Nabawy, et al. 2021). The high flexibility of the flag needed for the large amplitude flapping mode means sacrificing elasticity. This implies that recovering from full deflection to limit cycle flapping in a steady state is much harder, unless wind speed is reduced significantly.

In addition, once the flag has been fully deflected it experiences a much higher force from the oncoming flow than during the oscillation period. This means that even when the wind speed reduces to speeds that previously had oscillations, the restoring internal elastic force within the flag is not high enough to overcome the large drag force experienced.

It can also be seen that higher mass ratio flags have comparatively higher frequencies than their lower mass ratio counterparts, even though all dimensions apart from thickness are the same. This phenomenon can be attributed to how the elastic restoring force changes with thickness. As all dimensions regarding the interaction with the oncoming flow are the same (i.e. C_r , C_t , planform area and L), the experienced fluid force is the same between all flags. However, with extra thickness, the restoring elastic force increases, thus driving the flag to return to the equilibrium position at a faster rate.

The effects of mass ratio have not been studied extensively in previous literature (at least not to the findings of this project). However, the findings here agree with the results found in both Yang, Nabawy, et al. 2021 and Kim et al. 2013, thus concluding that the effects of mass ratio are consistent between rectangular and tapered flags.

5.2 Taper Ratio Investigation

In the following section the general behaviour of tapered flags is outlined and discussed, as well as the dynamical effects of taper on inverted flags. The main dynamic states of motion described in Section 2 were observed in four out of five of the flags tested (those being F1 - F4), whilst F5 did not show full deflection. As discussed in Section 5.1 each flag has an onset velocity (U_{onset}) at which limit cycle flapping occurs and the flag becomes unstable. At a certain velocity the flag begins to exhibit chaotic motion (part way between flapping and full deflection), and then eventually is fully deflected (U_{offset}). The corresponding onset, offset, and working ranges are shown in Table 4.

Table 4: Dynamics characteristics of each tapered flag for overall measurements. U_{Stop} is the wind speed at which the flag transitioned from limit cycle flapping to rest.

Average Performance							
Flag	μ	U_{Onset} [ms $^{-1}$]	U_{Offset} [ms $^{-1}$]	U_{Range} [ms $^{-1}$]	U_{Stop} [ms $^{-1}$]	θ_{Avg} [$^{\circ}$]	F [Hz]
F1	8.485	10.03	18.02	7.99	8.79	169.6	8.00
F2	6.717	9.05	13.74	4.69	9.22	152.59	3.85
F3	4.837	NA	9.31	NA	4.82	130.42	2.13
F4	5.435	10.26	11.53	1.27	5.7	185.24	4.29
F5	8.584	21.11	NA	NA	12.62	138.3	13.60

Figure 23 shows the measurement results of the tapered flags. Figure 23 (a) shows the frequency whilst (b) shows the angular amplitude for both increasing and decreasing wind speeds. As mentioned in Section 5.1, measuring results for both increasing and decreasing wind speeds allows for the

identification of any hysteresis. In Figure 23 a strong correspondence between the increasing and decreasing wind speeds is observed.

However, there is a clear difference between the transition speeds for flapping to deflection in the increasing velocity, and vice versa in decreasing velocity tests. Whilst the hysteresis was expected (Kim et al. 2013, Sader, Cosse, et al. 2016, Sader, Huertas-Cerdeira, and Gharib 2016, Yang, Nabawy, et al. 2021 etc.) the effects shown in Figure 23 are far more pronounced than those shown in Figure 6.

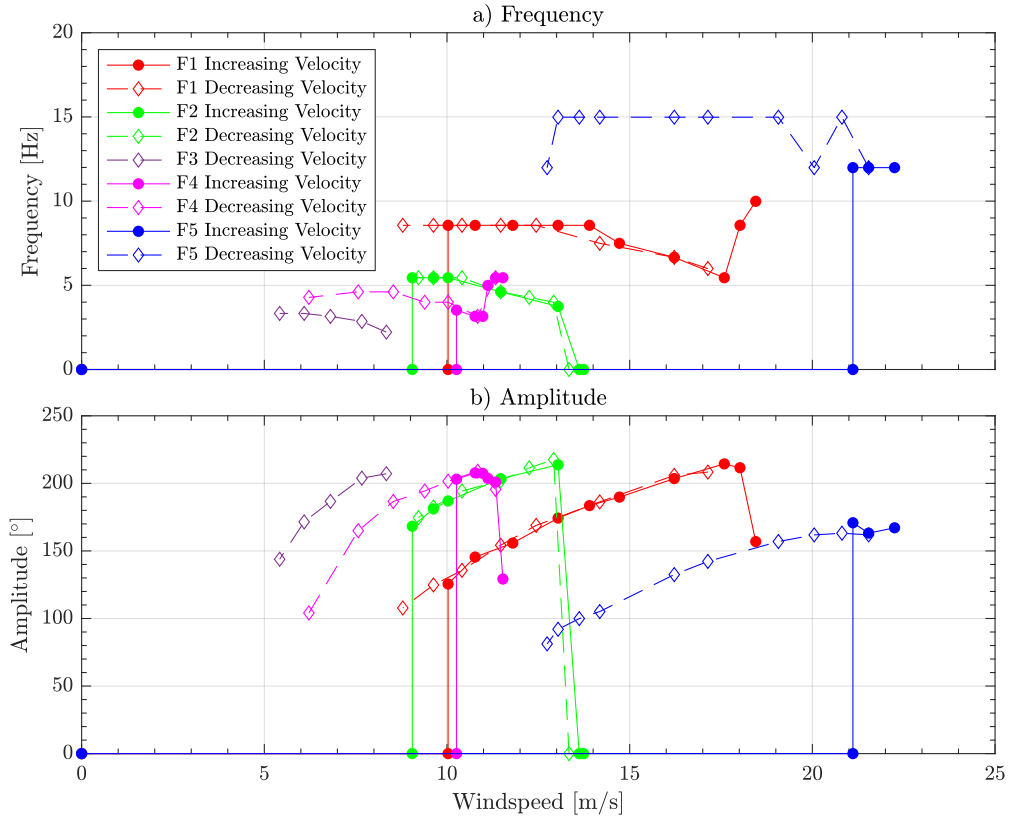


Figure 23: Taper ratio test flags. Plotting Wind speed [ms^{-1}] against Frequency [Hz] and Amplitude [$^{\circ}$]

As mentioned in Section 3.2, each of the original sheets the flags were manufactured from showed residual deformation due to the manner in which they were stored. This initial curvature created an inherent bias within the structure of the flag regarding the direction in which initial deformation would occur (i.e. which direction the flag would start flapping first). As such, more energy (equating to a higher onset flow velocity) is required to initiate transition between flapping regimes. This can clearly be seen in Figure 23 as each of the flags transition to limit cycle flapping at a later stage than when the flag returns from flapping to no deflection. Flag F3 in particular did not even exhibit flapping on increasing wind velocities at all, transitioning directly to full deflection before returning to flapping in decreasing wind speeds.

It is also evident that those flags with sub 1 taper ratios have extra difficulty transitioning from rest to flapping at lower wind speeds. This could be attributed to how and where the lift force varies and is generated over the flag. The majority of the lifting force which initiates the flapping is generated at the leading edge of the flag. As these $\lambda < 1$ flags have a comparatively smaller leading edge compared to other flags, they generate less lifting force at the same wind speeds. The trailing edge is also larger in comparison to the leading edge. In previous literature, typically the C_r and C_t have been equal

lengths, whereas here because of the difference in lengths, the ratio of lift to the structural rigidity it has to overcome is also higher, leading again to higher onset wind speeds to initiate flapping.

It is evident from Figure 23 that those flags with the more extreme tapers exhibit higher frequencies in the limit cycle flapping period. Both F1 and F5 clearly have the highest flapping frequencies and average 8.00 Hz and 13.6 Hz respectively (Table 4). Arguably, these two flags exhibit higher frequencies for opposite reasons, with F1 most likely being the high lift and drag forces compared to the restoring force at the root, whilst F5 having an overwhelming restoring force compared to the lift and drag forces. Along with these two flags having the highest mass ratio out of the flags tested, this could also be the reason that the two oscillate at higher wind speeds.

Apart from F5, each flag exhibits relatively similar maximum and minimum amplitudes across the set, ranging from $100^\circ - 200^\circ$. Each flag shows a relatively similar trend, in a non-linear increase/decrease in amplitude as wind speed increases/decreases respectively. Considering the constant AR of 0.75, and comparing to the results from Yang, Nabawy, et al. 2021 in Figure 7, these results are relatively consistent with previous literature.

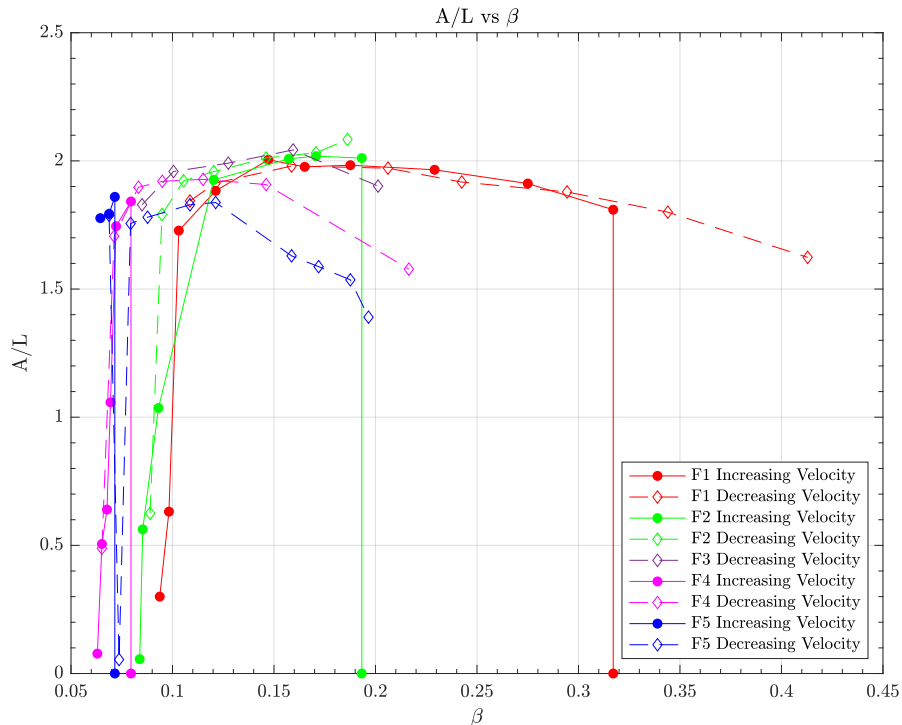


Figure 24: Taper ratio test flags. Plotting A/L vs β for increasing and decreasing wind speeds.

Regarding Figure 24, there are similarities and differences between the results displayed, and those in other literature such as Kim et al. 2013, whose results are shown in Figure 6. The range of A/L exhibited was relatively similar, but slightly higher. Whilst Kim et al. 2013 found a range of $\sim 1.7 - 1.8$ the range for the inverted flags is $\sim 1.7 - 2.0$, showing slightly higher/deflection compared to the overall length of the flag. Each flag quickly reaches this range upon increasing and decreasing wind speeds, before plateauing within the shown range. This higher A/L does not necessarily equate to higher actual deflection or more strain energy at the root. This is based on the amplitude data shown in Figure 23.

Unlike previous studies, the range of β in which flapping occurs is inconsistent between flags of differing geometry. All but one of the flags flap between approximately $0.075 < \beta < 0.225$, apart from F1, which

flaps between $0.025 < \beta < 0.31$ (0.425 for decreasing velocity increments). This differs greatly from previous observed trends which show rectangular planform flags flapping in the range $0.1 < \beta < 0.3$. At this stage however, it is hard to conclude whether this effect is due to the taper of the flags, or is possibly an effect of the residual curvature present in each of the flags during the test, as discussed in previous sections.

5.3 Fluid Energy

Whilst there is no direct conversion from flapping amplitude or frequency to the energy that can be extracted, an analysis can be conducted based on the fluid energy imparted to the flag. A study was conducted by Tang, N. S. Liu, and Lu 2015 regarding the dynamics of inverted flexible plates in uniform flows. Part of the research conducted in this study was based on the conversion rate of fluid energy to strain energy within the flag. There is a subsequent conversion to electrical energy but this requires piezoelectric materials and there is no set function for this calculation.

The following equation was derived to find the ratio of fluid kinetic energy to the bending energy of the plate:

$$E_R = \frac{E_{Bmax}}{0.5\rho U^3 |x| W \hat{T}} \quad (5)$$

Where E_{Bmax} is the maximum bending energy during flapping, ρ is the fluid density, U is the fluid flow velocity, $|x|$ is the maximum transverse displacement (essentially the non-angular amplitude), W is the tip length (C_t), and \hat{T} is the time taken from rest to maximum displacement. The denominator of the shown equation correlates to the kinetic energy of the oncoming flow passing through the maximum frontal area during the time interval. The energy expended by the flow was calculated using the denominator. The results for all tapered flags for both increasing and decreasing velocity increments is shown in Figure 25. The function used to is shown in Appendix B.

As expected, the tapered flags required more energy to induce flapping due to the variances in the elastic restoring force, lift, and drag as previously discussed in Section 5.2. The more extremely tapered flags also experience more energy imparted to their surface due to the increased wind speeds and previously discussed effects of λ . In the mentioned study (Tang, N. S. Liu, and Lu 2015), the aspect ratios studied were $AR = 0.5, 1.0, 1.5$ and 2.0 , with approximately $17\% - 18\%$ of the fluid kinetic energy being converted into bending energy. Taking the assumption that this conversion rate would also apply to tapered flags, the corresponding adjusted data is shown in Figure 26.

As expected, each flag experiences more fluid energy as wind speed increases, due to the cubic term in Equation 5. Each flag follows a relatively similar trend in terms of the fluid energy imposed onto the surface, reinforcing that the dominant term is the wind speed. Subsequently looking at Figure 26 is also the dominant factor in the bending energy generated within the flag during deformation. Flags F1-F4 all require relatively similar energy levels in the fluid to transition either from rest to limit cycle flapping, or vice versa. They only seem to separate in the energy levels required as the higher wind speeds are reached. Where some flags (F3 and F4) fully deflect, others (F1 and F2) have enough rigidity within themselves to withstand the higher wind speeds, and still flap under the higher energy levels.

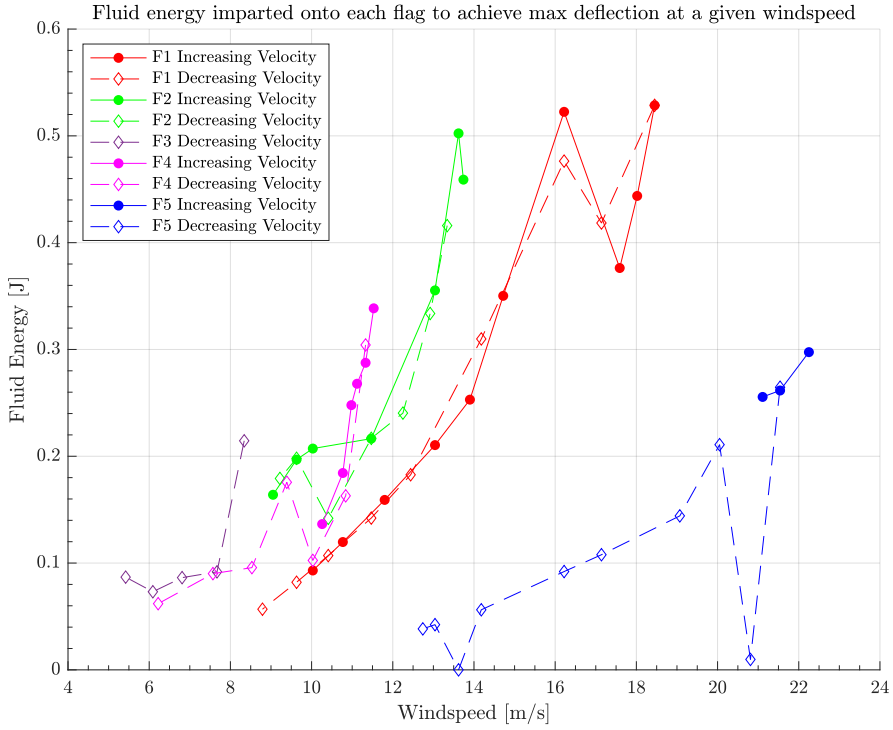


Figure 25: Fluid energy imparted onto the surface of the flag to reach the maximum flapping amplitude at a given windspeed.

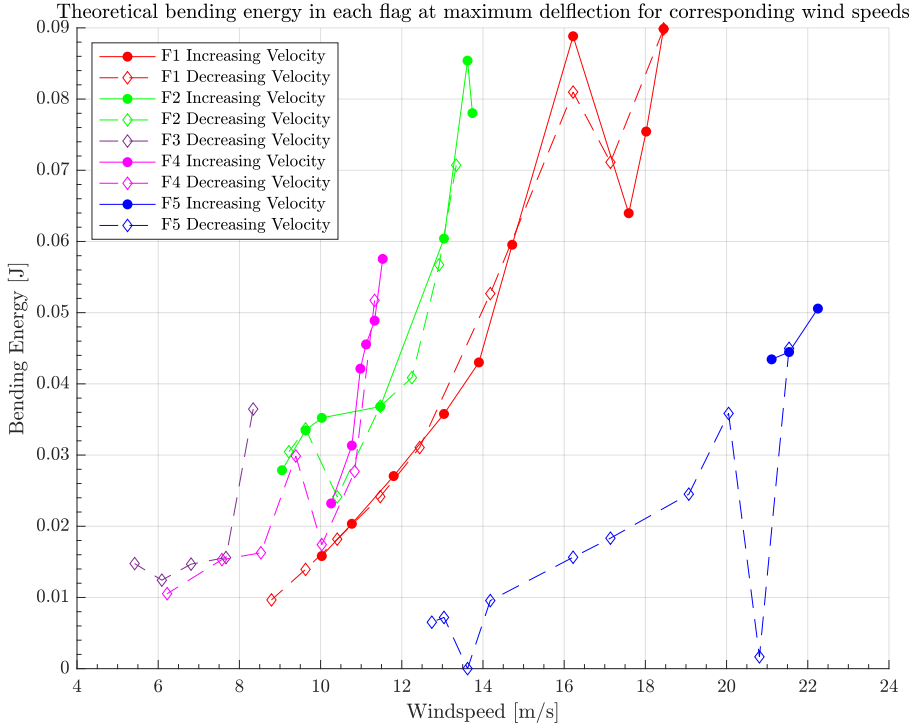


Figure 26: Theoretical bending energy generated in each flag at maximum deflection for a given wind speed.

Flag F5 is a clear outlier to the general behaviour followed by the other flags (this is also shown in Figures 23, 23). It does follow a relatively similar trend in the increasing flow energy levels, however the magnitude is significantly reduced, and the rate of increase is also lower despite it being geometrically the same as F1 in all aspects except orientation. However, looking at Table 3 and Figure 23 the flapping frequency of F5 is significantly higher than all other flags. This reason is due to the orientation and how that effects the lift to structural rigidity ratio, and has been discussed in more depth in Section 5.2.

The comparatively higher frequency results in a lower period of oscillation, thus significantly reducing the \hat{T} term in Equation 5. This leads to a reduction in the energy passed between the fluid and the surface of the flag.

Whilst converting the fluid kinetic energy to bending energy generated can be useful as in Figure 26, it is not actually representative of the energy that could be extracted from the flag. That depends on the piezoelectric materials used, their efficiency and configuration on the flag surface. It also depends on their efficiency, as well as how the combining of two different materials with different properties will effect the behaviour of the flag. There is currently no known way to define overall material properties when combining two dissimilar materials in this way, consequently there is no equation or direct translation from bending or fluid energy to the energy that can be generated by the flag itself. It is also worth noting that $|x|$ displacement is not the only factor that effects the energy that can be extracted. Whilst flapping is relatively symmetrical, there is asymmetrical displacement in the y axis. Some flags part way through an oscillation may form and 's' shape, possibly cancelling charge between piezoelectric strips, or the displacement in y may be greater than that in x , but Equation 5 does not account for this.

6 Conclusions, Limitations, and Further Work

6.1 Conclusion

The objective of this project was to investigate the effect of taper on the dynamics of inverted flags. Inverted flags are becoming a popular area of research regarding power generation for small scale portable electronics, such as remote sensors. Different flags with different values of λ will behave very differently to each other, with the more extreme tapers exhibiting higher flapping frequencies than their less tapered counterparts. As well as this, they generally oscillate at higher wind speeds. Flags with values of $\lambda < 1$ tend to struggle more with transitioning to limit cycle flapping on the increasing wind speeds, but once they have transitioned show some of the largest ranges of effective working speeds.

Tapered flags also average higher relative deformations than standard inverted flags, as shown by Figure 24, but seem to oscillate for a lower range of β . However, it is unclear at this point how much of this is due to the residual deformation and stresses in the material present from shipping (this also applies to the exaggerated hysteresis shown in Figure 23).

6.2 Research Question

The end goal of this project was to ascertain whether the extra effort and associated cost of producing tapered inverted flags for energy harvesting is worth it. Without more research, it is not practical to provide an answer at this stage. Whilst the initial results are promising in the frequency and amplitude respects, the more irregular shape of the planform would have an effect on the number of piezoelectric materials that could be attached to the surface, and thus the energy that could be extracted from the flag. Additionally, combining two different materials has an effect of the associated properties, and as of yet there is no known way to come to a final value for density, young's modulus etc.

However, the results shown are relatively similar, but slightly higher, than those shown in previous

literature, so whilst promising, it is not a definitive answer that tapering inverted flags provides any substantial additional benefits.

6.3 Limitations and Future Work

In this section, limitations of the experiments performed are outlined and discussed, as well as what should be done in future to improve the quality of results gained, and to provide a more definite answer to the original research question. There are two main areas of focus, the materials used, and translating the results gained to estimations for power output.

6.3.1 Materials Used and Manufacturing

As discussed in previous sections, the materials for the flags arrived rolled, causing there to be some pre-existing deformation in the flags. Several methods were attempted to rectify this, however they proved unsuccessful. This most likely contributed to the hysteresis shown in the results, and the difficulties some flags exhibited in transition from straight to limit cycle flapping, but without further testing it cannot be certain. To verify this, sources of the same material, but shipped in flat sheets instead of rolled, should be found. Then flags of the same dimensions listed can be manufactured and tested under the same conditions, and the results compared to those outlined in this paper to see if the same hysteresis effect is present.

6.3.2 Energy Harvesting

In the literatures reviewed, due to the unknown effect of combining two materials on the overall material properties, there is no set formula to be able to translate frequency and amplitude to the possible power generated. Without attaching piezoelectric materials to the surface of the flag, this number will remain unknown. In future, once the material issues have been solved, these tests should be performed again with piezoelectric materials. Additionally this different layouts of said materials may be more optimal than others. Whilst in previous literature the layout has been consistent with those shown in Yang, Nabawy, et al. 2021, due to the nature of the planform of a tapered flag this layout may not be possible. Subsequently, there may be differing layouts that provide more efficient energy production.

References

- 302 Stainless Steel (n.d.). URL: https://www.matweb.com/search/datasheet_print.aspx?matguid=05efb28c10154f2796f4bf033363880a.
- Connell, Benjamin S.H. and Dick K.P. Yue (June 2007). “Flapping dynamics of a flag in a uniform stream”. In: *Journal of Fluid Mechanics* 581, pp. 33–67. ISSN: 1469-7645. DOI: [10.1017/S0022112007005307](https://doi.org/10.1017/S0022112007005307). URL: <https://www.cambridge.org/core/journals/journal-of-fluid-mechanics/article/flapping-dynamics-of-a-flag-in-a-uniform-stream/D706FD7A792F75287A1766434ADF485F>.
- Fan, Boyu et al. (2019). “Effect of morphology on the large-amplitude flapping dynamics of an inverted flag in a uniform flow”. In: *Journal of Fluid Mechanics* 874, pp. 526–547. ISSN: 0022-1120. DOI: [10.1017/JFM.2019.474](https://doi.org/10.1017/JFM.2019.474). URL: <https://www.cambridge.org/core/journals/journal-of-fluid-mechanics/article/effect-of-morphology-on-the-largeamplitude-flapping-dynamics-of-an-inverted-flag-in-a-uniform-flow/599C09DC83303FAD5128B2EABF2327EF>.
- “GLOBAL CLIMATE” (Aug. 2022). In: *Bulletin of the American Meteorological Society* 103 (8), S11–S142. ISSN: 15200477. DOI: [10.1175/BAMS-D-22-0092.1](https://doi.org/10.1175/BAMS-D-22-0092.1).
- Gurugubelli, P.S. and R.K. Jaiman (2019). “Large amplitude flapping of an inverted elastic foil in uniform flow with spanwise periodicity”. In: *Journal of Fluids and Structures* 90, pp. 139–163. DOI: [10.1016/j.jfluidstructs.2019.05.009](https://doi.org/10.1016/j.jfluidstructs.2019.05.009). URL: <https://doi.org/10.1016/j.jfluidstructs.2019.05.009>.
- Hansen, James et al. (Dec. 2013). “Assessing “Dangerous Climate Change”: Required Reduction of Carbon Emissions to Protect Young People, Future Generations and Nature”. In: *PLOS ONE* 8 (12), e81648. ISSN: 1932-6203. DOI: [10.1371/JOURNAL.PONE.0081648](https://doi.org/10.1371/JOURNAL.PONE.0081648). URL: <https://journals.plos.org/plosone/article?id=10.1371/journal.pone.0081648>.
- Irrigation Scheduling Using Soil Water Tension Sensors - Alabama Cooperative Extension System* (n.d.). URL: <https://www.aces.edu/blog/topics/crop-production/irrigation-scheduling-using-soil-water-tension-sensors/>.
- Kerr, Jeremy T. and Marsha Ostrovsky (June 2003). “From space to species: Ecological applications for remote sensing”. In: *Trends in Ecology and Evolution* 18 (6), pp. 299–305. ISSN: 01695347. DOI: [10.1016/S0169-5347\(03\)00071-5](https://doi.org/10.1016/S0169-5347(03)00071-5). URL: [http://www.cell.com/article/S0169534703000715/abstract%20https://www.cell.com/trends/ecology-evolution/abstract/S0169-5347\(03\)00071-5](http://www.cell.com/article/S0169534703000715/fulltext%20http://www.cell.com/article/S0169534703000715/abstract%20https://www.cell.com/trends/ecology-evolution/abstract/S0169-5347(03)00071-5).
- Kim, Daegyoun et al. (2013). “Flapping dynamics of an inverted flag”. In: *J. Fluid Mech* 736, p. 1. DOI: [10.1017/jfm.2013.555](https://doi.org/10.1017/jfm.2013.555). URL: <https://doi.org/10.1017/jfm.2013.555>.
- Kornecki, A., E. H. Dowell, and J. O’Brien (July 1976). “On the aeroelastic instability of two-dimensional panels in uniform incompressible flow”. In: *Journal of Sound and Vibration* 47 (2), pp. 163–178. ISSN: 0022-460X. DOI: [10.1016/0022-460X\(76\)90715-X](https://doi.org/10.1016/0022-460X(76)90715-X).
- Lannoy, Steven De (2014). *Wing Bending Calculation with a Single set of Equations*.
- Ojo, Oluwafemi et al. (Mar. 2019a). “Aspect ratio effects in wind energy harvesting using piezoelectric inverted flags”. In: *SPIE* 10967, 109670Q. ISSN: 1996756X. DOI: [10.1117/12.2519527](https://doi.org/10.1117/12.2519527). URL: <https://ui.adsabs.harvard.edu/abs/2019SPIE10967E..0Q0/abstract>.

- Ojo, Oluwafemi et al. (Mar. 2019b). “Aspect ratio effects in wind energy harvesting using piezoelectric inverted flags”. In: *SPIE* 10967, 109670Q. ISSN: 1996756X. DOI: [10.1117/12.2519527](https://doi.org/10.1117/12.2519527). URL: <https://ui.adsabs.harvard.edu/abs/2019SPIE10967E..0Q0/abstract>.
- Orrego, Santiago et al. (May 2017). “Harvesting ambient wind energy with an inverted piezoelectric flag”. In: *Applied Energy* 194, pp. 212–222. ISSN: 0306-2619. DOI: [10.1016/J.APENERGY.2017.03.016](https://doi.org/10.1016/J.APENERGY.2017.03.016).
- Sader, John E., Julia Cosse, et al. (Apr. 2016). “Large-amplitude flapping of an inverted flag in a uniform steady flow – a vortex-induced vibration”. In: *Journal of Fluid Mechanics* 793, pp. 524–555. ISSN: 0022-1120. DOI: [10.1017/JFM.2016.139](https://doi.org/10.1017/JFM.2016.139). URL: <https://www.cambridge.org/core/journals/journal-of-fluid-mechanics/article/largeamplitude-flapping-of-an-inverted-flag-in-a-uniform-steady-flow-a-vortexinduced-vibration/388AEE925ABB33381CEE0157F32737DF>.
- Sader, John E., Cecilia Huertas-Cerdeira, and Morteza Gharib (Dec. 2016). “Stability of slender inverted flags and rods in uniform steady flow”. In: *Journal of Fluid Mechanics* 809, pp. 873–894. ISSN: 0022-1120. DOI: [10.1017/JFM.2016.691](https://doi.org/10.1017/JFM.2016.691). URL: <https://www.cambridge.org/core/journals/journal-of-fluid-mechanics/article/stability-of-slender-inverted-flags-and-rods-in-uniform-steady-flow/CFDF5240DA89FEBEFFB73A5431F2C0DA>.
- Silva-Leon, Jorge et al. (Apr. 2019). “Simultaneous wind and solar energy harvesting with inverted flags”. In: *Applied Energy* 239, pp. 846–858. ISSN: 0306-2619. DOI: [10.1016/J.APENERGY.2019.01.246](https://doi.org/10.1016/J.APENERGY.2019.01.246).
- Sishodia, Rajendra P., Ram L. Ray, and Sudhir K. Singh (Sept. 2020). “Applications of Remote Sensing in Precision Agriculture: A Review”. In: *Remote Sensing 2020, Vol. 12, Page 3136* 12 (19), p. 3136. ISSN: 2072-4292. DOI: [10.3390/RS12193136](https://doi.org/10.3390/RS12193136). URL: <https://www.mdpi.com/2072-4292/12/19/3136>.
- Taneda, Sadatoshi (1968). “Waving Motions of Flags”. In.
- Tang, Chao, Nan Sheng Liu, and Xi Yun Lu (July 2015). “Dynamics of an inverted flexible plate in a uniform flow”. In: *Physics of Fluids* 27 (7). ISSN: 10897666. DOI: [10.1063/1.4923281](https://doi.org/10.1063/1.4923281).
- Tavallaeinejad, Mohammad, Michael P. Païdoussis, et al. (2020). “Instability and the post-critical behaviour of two-dimensional inverted flags in axial flow”. In: *Journal of Fluid Mechanics* 890. ISSN: 14697645. DOI: [10.1017/jfm.2020.111](https://doi.org/10.1017/jfm.2020.111).
- Tavallaeinejad, Mohammad, Manuel Flores Salinas, et al. (2021). “Dynamics of inverted flags: Experiments and comparison with theory”. In: *Journal of Fluids and Structures* 101. DOI: [10.1016/j.jfluidstructs.2020.103199](https://doi.org/10.1016/j.jfluidstructs.2020.103199). URL: <https://hal.science/hal-03124681>.
- “The Carbon Cycle” (2011). In.
- Turner, Woody et al. (June 2003). “Remote sensing for biodiversity science and conservation”. In: *Trends in Ecology and Evolution* 18 (6), pp. 306–314. ISSN: 01695347. DOI: [10.1016/S0169-5347\(03\)00070-3](https://doi.org/10.1016/S0169-5347(03)00070-3).
- Yang, Kaidong, Andrea Cioncolini, et al. (Dec. 2023). “Wind Energy Harvesting with Vertically Aligned Piezoelectric Inverted Flags”. In: *Sensors* 23 (24). ISSN: 14248220. DOI: [10.3390/s23249673](https://doi.org/10.3390/s23249673).
- Yang, Kaidong, Mostafa R A Nabawy, et al. (2021). “Planform geometry effects of piezoelectric wind energy harvesting composite inverted flags”. In: DOI: [10.1088/1361-665X/ac2b8a](https://doi.org/10.1088/1361-665X/ac2b8a). URL: <https://doi.org/10.1088/1361-665X/ac2b8a>.

Yu, Yuelong, Yingzheng Liu, and Xavier Amandolese (Jan. 2019). “A Review on Fluid-Induced Flag Vibrations”. In: *Applied Mechanics Reviews* 71 (1). ISSN: 00036900. DOI: [10.1115/1.4042446](https://doi.org/10.1115/1.4042446) / 368819. URL: <https://dx.doi.org/10.1115/1.4042446>.

7 Appendix A: Initial Project Plan and Proposal

7.1 Project Proposal

The initial proposal for this project was simply to investigate how taper ratio effects the critical wind speeds for flapping regime transition. Whilst to an extent this is still true, however the original plan was based on limited knowledge and flawed understanding of the governing parameters of inverted flags. Extensive literature review has revealed that whilst at the base level, different wind speeds induce different behaviour, every single flag will produce different behaviour at varying wind speeds. It is therefore better to quantify behaviour using non-dimensional parameters bending stiffness β and mass ratio μ , as well as using flapping frequency and amplitude. The initial Gantt chart for the initial project proposal is in Figure 27.

Teaching Weeks of Semester 1	1	2	3	4	5	6	7	8	9	10	11	12
Project Milestones Due												
Initial Project Objectives		█										
Project Proposal Report						█	█					
Other Course Deadlines												
Control Systems Engineering Coursework					█	█						
Aerodynamics Courseworks			█	█		█	█		█	█		
CASD Initial Report					█	█						
CASD tradeshow poster								█				
CASD Individual report										█		
CASD Final Report											█	
Aeroelasticity Coursework						█						
Aeroelasticity Report (Unknown)												
Operations Management (Ongoing)												
Work Packages												
Literature Review			█	█	█	█						
Writing Project Proposal					█	█						

Figure 27: Gantt chart in the initial project proposal, red cells signify due dates.

7.2 Methodology

7.2.1 Proposed Experiments

As outlined Section 2, different planform geometry changes have different effects on the behaviour of inverted flags, as such, multiple experiments will be required to find optimal geometries based on taper ratio. The first set of experiments will be solely focused on the effect of taper ratio alone. Aspect ratio will be a fixed value, and taper ratio will vary between $X < \lambda < Y$ in increments of Z . Mass ratio will not be kept constant, thickness will be kept constant.

The purpose of this experiment is to determine the effects of taper ratio alone. Each flag of a given taper ratio will be subject to a range of wind speeds. The experiment will be recorded with a high speed camera (yet to define) and then processed using MATLAB to find the flapping amplitude and frequency for given wind speeds and taper ratios. After the results of this experiment have been analysed three taper ratios will be chosen for further study based on their average values of amplitude and frequency to study the effects of mass ratio on behaviour. As aspect ratio and taper ratio will be fixed, the only way of varying the mass ratio will be by varying the thickness of the flag, typical thicknesses are around 0.2, 0.4, and 1 mm so the experiment will be constrained to three different mass ratios. This will result in 9 different flags being tested (3 taper ratios, 3 mass ratios per taper ratio). This will allow us to compare with other studies on the effect of mass ratio and determine if the effect is the same when the flag is tapered.

7.2.2 Experimental Design

The proposed experiments in section 7.2.1 will require more research and hands on learning to fully define, as such the steps below will be taken to ensure their reliability:

1. Establish base parameters, i.e visiting the wind tunnel lab to take measurements on the test sectional area and see the methods available for suspending an inverted flag in the test section.
2. Research the materials available, does the university already have appropriate shims, or will research need to be conducted on commercially available materials.
3. Design and manufacture a clamp, if one is not already available, that will be able to appropriately hold an inverted flag in the test section.
4. Consider taper and aspect ratios possible based on the dimensions of the test section and the materials available. It's possible length may have a constraint or depth will have constraints to be considered, affecting the possible ratios for testing.
5. Design an array of flags for the first experiment proposed in section 7.2.1.
6. Test said flags in the wind tunnel, recording footage at all wind speeds.
7. Analyse the data recording peak and average amplitudes and frequencies for each taper ratio.
8. Use the data to design a new array of flags for the second experiment proposed in section 7.2.1.
9. Repeat steps 6 and 7 but for mass ratio.

7.2.3 Performance Metrics

Throughout this study, the metrics used to quantify performance will be flapping frequency, and the flapping amplitude. Whilst this paper does not study the amount of power generated by a tapered inverted flag, these two metrics are the primary governing factors when apply piezoelectric materials to the flag. High amplitude flapping will produce large strains near the clamped base of the flag, thus any piezoelectric materials bonded to the flag will produce more power. Higher flapping frequencies will increase how often the piezoelectric materials are producing power, a higher frequency is better.

It may be that with taper ratio that both frequency and amplitude cannot be increased at the expense of the other, as such, regardless of the outcome, a critical discussion will ensue on the performance of the two. As well as this it will also be necessary to discuss how the changing planform area will affect the power generation capabilities, it may be that a high taper ratio produces better values of flapping frequency and amplitude, but this decreases the effective area to place piezoelectric strips, especially at the base where the highest strain energy will occur.

8 Project Planning

8.1 Semester 1

For the duration of Semester 1 the primary focus lies in the development of understanding how inverted flags behave and why, as well as planning experiments and fabricating the flags that will be tested.

This was achieved by undertaking a thorough review of previous literature written on the subject, and will be achieved by visiting the wind tunnel labs at the university. Work packages have been developed to organise and plan the semester efficiently, and dedicate time to the activities so far and the expected time it will take to finish them.

8.1.1 WP1 - Literature Review

The main focus this semester was to research and review the research that has been conducted thus far on inverted flags and their behaviour. Work started at the beginning of the semester by reading a few papers provided by the supervisor and supporting PhD student. These gave an initial understanding on the physics and governing factors of inverted flags, and provided a good baseline for further research. After a solid baseline understanding had been established, thorough research was undertaken to see what this sector of research was missing, and what could be contributed in this project. The main outputs of this work package were: overview of the existing literature, the studies conducted, their strong points and the areas where more research is required, and the future focus of this project.

8.1.2 WP2 - Hands-on Learning and Research

Visits to the wind tunnel labs will need to be undertaken in order to see the facilities available. An understanding of the systems will be required to fully develop each flag's dimensions and the system that will be used to clamp the flag at the trailing edge and point the leading edge into the wind. Meetings with staff at the university will also be required regarding the materials available for fabricating the flag, dimensions and material properties will be needed, and if required there may be necessary research into finding commercially available materials if the university is not adequately stocked.

8.1.3 WP3 - Project Proposal

The project proposal was written in conjunction with the literature review. This was necessary to be able to derive the experiments that would take place, in order to be able to justify the decisions made in the planning process. Notes and summaries were created of numerous papers on different subject areas within the study of inverted flags. These findings were then compared and summarised in the literature review in section 2, and the final project proposal was formed.

8.1.4 WP4 - Design and Fabrication

To allow for as much time as possible for testing and analysis in Semester 2, it would be ideal if the design fabrication of a clamping system (if necessary) and the inverted flags were completed in Semester 1. Knowledge from the previous work packages in sections 8.1.1, 8.1.2 and 8.1.3 will be brought together to finalise all the dimensions of the flags to be tested. Material properties will be recorded to include in the final report and to use for calculations. Some aspects of work package 4 will take place in Semester 2, as the results of the first experiment will affect the geometries tested for the second experiment.

8.1.5 Semester 1 Gantt Chart

The Semester 1 Gantt chart (Figure 28) includes all the work packages intended to carry out within the current semester, and all other deadlines for other course units. An important note is whilst the

literature review is being submitted in this submission, work will continue on it for the remainder of the semester to improve upon what is already written, and if new literature is found this will be included in time. Work on the literature review is planned to finish by the Christmas break.

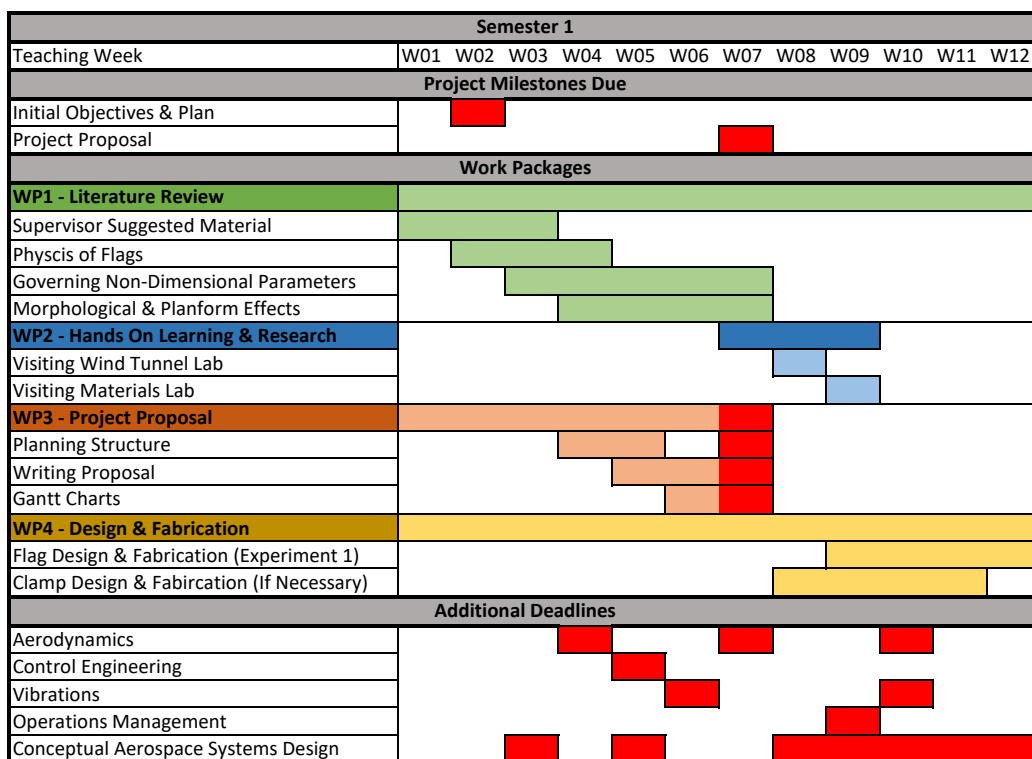


Figure 28: Semester 1 Gantt Chart and Planning. Red cells signify due dates.

8.2 Semester 2

For the duration of Semester 2, the primary focus will be to apply the knowledge gained in Semester 1, test different geometries of inverted flags, and compile the results into the deliverables required. Both the poster and final report will be written in tandem with the data collection and analysis. The time allocated to each activity should allow for sufficient time to complete the project deliverables.

8.2.1 WP5 - Testing

This work package should take the least amount of time, and in theory can be completed in two to three days depending on any delays. As with the nature of the experiments it won't be possible to do all the testing required on the same day, but each set of testing should take no more than a day. The first set of testing shall be completed as early in the semester as possible. Once the first test is completed, results will be analysed, and specific planform geometries will be chosen for the next set of testing. Within this time frame work will also be completed on the poster and final report.

8.2.2 WP6 - Work on Deliverables

There are 3 main deliverables throughout Semester 2: poster submission, poster presentation, and the final report. The poster submission is essentially a summary of the research topic, its background, aims, and methodologies, as well as any results already collected, and any results left to collect. It will be captured in A1 paper size and presented to the project supervisor and another assessor on the poster presentation day in Week 6 of Semester 2 (the poster itself will be submitted in

Week 4W). It is worth noting there is a formative deliverable of a Writing Sample due in Week 8 of Semester 2, but this is formative and does not need separate consideration as the content will be written as part of the final report. The final deadline is the final report due in Week 11. This will take a considerable amount of time, hence it is proposed to start in Week 5 in order to leave enough time to deliver in Week 11. Whilst there is small overlap between working on all these deliverables, they are kept relatively separate to ensure a high level of quality throughout.

8.2.3 Semester 2 Gantt Chart

The Semester 2 Gantt chart outlines the intended timeline for the relevant work packages, deadlines for Semester 2 courses are not available yet and as such have not been included. If the available times for using the wind tunnel are not in line with the plan then the plan will change.

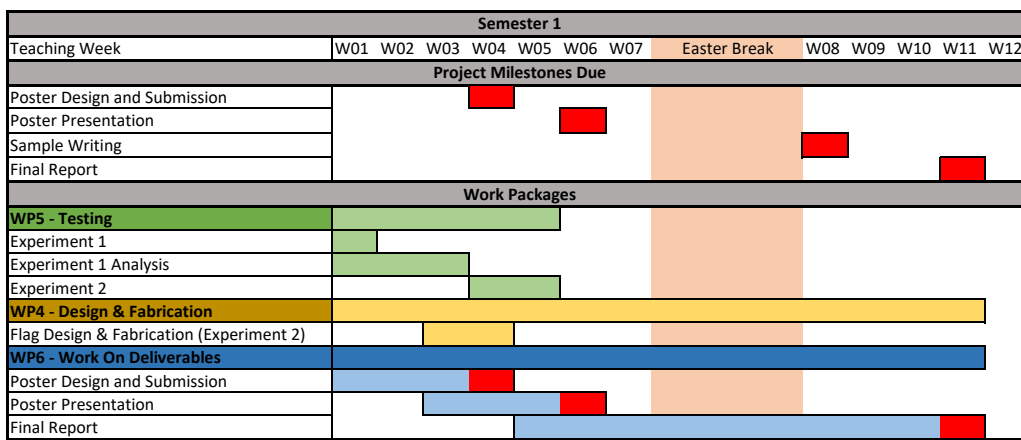


Figure 29: Semester 2 Gantt Chart and Planning. Red cells signify due dates. Other course deadlines are left out as they are not available yet.

9 Critical Reflection

9.1 Table of Risks

Risk	Likelihood	Severity	Mitigation	Progress
Not enough lab/access time	Medium	High	Begin testing as early as possible	None
Flags break	Medium	Medium	Possibly make multiple of each flag (dependent on materials)	None
Broken equipment	Low	High	Begin early to allow time	None
Time management	Medium	Medium	Follow proposed Gantt Chart, adapt quickly, make weekly "to do" lists	In Progress
Not enough materials	Medium	High	Confer with university as early as possible on resources available	In Progress

Table 5: Risks to current project plan.

In Table 5 there is a brief outline of the primary risks that will effect the timeline or outcome of this project. In this section each will be briefly discussed regarding their impact and possible mitigation techniques.

9.2 Not Enough Lab Access/Time

The university only posses a set amount of wind tunnels that will be appropriate for this project. Many academics and students at the university will also be in need of using this same wind tunnel for their own work. This means that it may not be possible to book the time necessary at the required time to perform the experiments for this project. As nearly all the content of this project is reliant on the use of the wind tunnel and the data that will be gathered there, the majority of the progress planned to be made in Semester 2 will be delayed until accessing the wind tunnel is possible. The only way to mitigate this outcome is to prepare all the relevant materials for the experiments as soon as possible and then book time in the wind tunnel lab as early in the semester as possible, preferable within first week of the semester.

9.3 Flags Break

During the experiments it will be necessary to subject the flags to wind speeds high enough to fully deflect them around the clamped end. Depending on the material used this could lead to permanent deformation of the flag and render it useless in terms of repeating an experiment with it. A good experiment is generally conducted several times to find the average of the data and make sure that there are no anomalies within a test. This means that multiple of the same flags will be required to mitigate the risk of time delay if/when a flag either breaks or permanently deforms. If the flags did break and there were no spares to replace them then the experiment would be delayed until the flag can be replaced, which would also most likely lead to having to finish the experiment on a different day, which may not be possible depending on the availability of the wind tunnel lab.

9.4 Broken Equipment

This subsection refers to equipment such as the wind tunnel or camera used in the experiments. The likelihood of this happening is relatively low. The wind tunnel and camera will be handled with extreme care at all times by those involved with this project as their malfunction would delay the entire progress of the project until replacements or repairs could be sought. There is the risk that the wind tunnel breaks under the use and supervision of someone else but this is a risk that is outside of our control and is therefore something that has to be expected regardless of its likelihood and impact.

9.5 Time Management

Time management is extremely important for this project. Along with completing this project, time will also need to split across other modules and assessments. As such it extremely important that the project plan is kept to, ensuring the completion of deliverables in a timely manner. Each subsequent delay in work package completion will effect the following tasks, constraining the amount of time left to complete the deliverables. As such, the current project plan will be kept to unless uncontrollable

circumstances change the plan, and weekly "to do" lists will be formed with the objectives of the week.

9.6 Not Enough Materials

A visit to the materials lab at the university will be required to assess if there will be enough to cut all flag geometries without the ordering of new materials. If the university does possess enough then there should not be any time delay. If there is not enough material then new materials will have to be ordered from the same manufacturer to ensure homogeneity between all flags as much as possible. The amount of time that this could delay the project by is unforeseen and out of control, it is purely dependent on the supplier and how quickly they would be able to deliver. To mitigate this risk as much as possible, a visit to the materials lab at the university will need to happen as soon as possible, in case more materials need to be ordered.

10 Conclusions and Future Work

Previous literature on the behaviour of inverted flags subject to an oncoming flow were reviewed in Section 2 of this report. Non-dimensional governing parameters, as well as morphological and planform effects were the primary points of focus. This provided sufficient information to develop a research question. After this, a general methodology was formed, however there were key numbers missing from defining the geometries that will be used as this requires visits to the wind tunnel and materials labs. From there a detailed experimental plan and procedure was developed spanning the duration of the academic year. Fabrications and experiments were carefully planned to allow for enough time to work on the deliverables of Semester 2.

11 Semester 2 Gantt Chart and Project Reflection

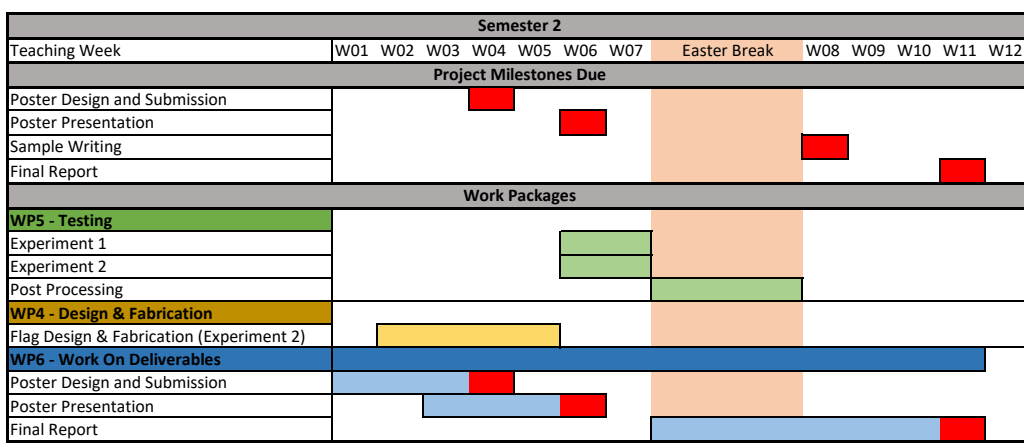


Figure 30: Revised semester 2 Gantt Chart and Planning. Red cells signify due dates. Other course deadlines are left out.

Shown in Figure 30 is a revised gantt chart of the semester 2 plan, based off of feedback on the previous project proposal and plan submission, as well as to account for any delays experienced. This section will outline the delays in the project that caused the plan to differ from those presented in Figure 29. There will also be a reflection on how the project could have been better managed, and any caveats that could be avoided by anyone endeavouring to undertake a similar project in the future.

The first delay was regarding obtaining the materials to manufacture the inverted flags from, and planning the geometries. Initially the plan was to have all geometries derived, and materials ordered, by the end of the first semester. However, deriving the geometries became more complicated than anticipated regarding separating as many variables as possible. I wanted to be able to only vary one parameter to see the direct effect, but unfortunately this was not possible, and a compromise had to be come to. This caused the flag design to be delayed until the second semester.

In terms or acquiring materials, cost suddenly became a large factor in the plan. Sheets of metal shim are relatively expensive, especially for the budget set by the University for third year projects. This mean Babar and myself had to collaborate to make our experiments and flags cut from the same sheets to share materials and drive down costs. This meant using the Christmas period and early second semester to find the correct materials from a reputable distributor/manufacturer, as ordering could not take place until we had calculated the area of material we would need to manufacture all the flags. Thankfully the chosen distributor had next day delivery so the delay was not substantial in the overall process.

Initially, it was planned that the mass ratio tests would take place first, and then I would come back after a period of post processing to test the flags designed for the taper ratio tests. However, as the project progressed it became apparent that this would take too much time, and it would instead be better to manufacture all flags and then test all together whilst the experimental setup was consistent. This meant that both experiments 1 and 2 were conducted in the same two weeks prior to the Easter break and then all post processing took place over the Easter break. This did not necessarily effect of the overall timeline, just the order in which a couple of work packages would take place.

I also experienced delays in the manufacturing period, due to the material defects described and discussed in Section 5.2. Solving the material defects took several efforts of trial and error in testing to find the best way to proceed. This meant delaying the experiments by a couple of weeks, however they still took place when intended, and if anything hindered being ahead of schedule if nothing else.

There was also an initial period of testing different experimental setups with the camera, wind tunnel, lighting, and then post processing, to find the most optimal setup we could for tracking the flags in post processing. This meant repeatedly testing flags and recording them, then trying to track and finding where the problems lay. This led to using a studio light to improve the lighting conditions, as well as the white background for the tracking video.

Gaining access to the wind tunnel lab earlier in the process would have also been beneficial. As mentioned in Section 3.3, the clamp that was originally designed was slightly too large for the wind tunnel in terms of length. Accessing the wind tunnel at an earlier stage would have allowed me to take measurements of the dimensions and see how the current clamp setup functioned. This would have meant that a more appropriate clamp could have been designed and manufactured. Whilst unlikely that the clamp had any significant effect (if any at all) on the results taken, it would have been an improvement regardless.

11.1 Project Management Reflection

Considering the changes to the semester two plan had relatively effect on the overall timeline of the project, I believe this project was relatively well planned from the start. The changes that happened came from general inexperience of conducting a project of this size and scope. However, I believe I adapted well and managed to keep on pace for deadlines. Once the plan had changed, each work package was completed by the intended deadlines shown in Figure 30.

Finishing the post processing over the Easter break allowed for ample time to write up the experimental procedure and the results in tandem with, and after the post processing had taken place, as the literature review had been completed during semester one. Aiming to complete the literature review in semester one was also a large part of the reason this project remained on schedule. This allowed total focus in semester two on the design, fabrication, testing of the flags, with a solid background on previous research.

In future, when planning another project of this scope, I would actually be less optimistic about how long each work package would take. Whilst some may seem simple to start with, the further you delve into the research, the more you find you did not see the first time. This causes delays in the initial plan as there is more work to complete than initially assumed. The plan should be based on encountering different unforeseen issues, and whilst unforeseen implies that we do not know of the issue beforehand, it is a safe assumption that issues will arise and the plan should be adjusted accordingly.

12 Appendix B: MATLAB Post-Processing

12.1 Frequency and Amplitude Calculation Function

```
1 function [Frequency, Amplitude, Amplitude2] = get_Freq_Amp(Time, x, y,
   A, B, C, D)
2
3 Theta = zeros(height(Time), 1);
4
5 for i = 1:height(Time)
6   if x(i) > 0 && y(i) > 0
7     Theta(i,1) = rad2deg(atan(x(i)/y(i)));
8   elseif x(i) < 0 && y(i) > 0
9     Theta(i,1) = -rad2deg(atan(x(i)/y(i)));
10  elseif x(i) < 0 && y(i) < 0
11    Theta(i,1) = 90 + rad2deg(atan(y(i)/x(i)));
12  elseif x(i) > 0 && y(i) < 0
13    Theta(i,1) = 90 + rad2deg(atan(abs(y(i))/x(i)));
14  end
15 end
16
17 Theta = 2 * Theta;
18 pk = findpeaks(Theta);
```

```

19 Amplitude = mean(pks);
20
21
22 t_axis = linspace(min(Time), max(Time), height(Time));
23
24 if isempty(A)||isempty(B)||isempty(C)||isempty(D)
25     [matlab_sine_wave,~] = fit(Time, x, 'sin1');
26     final_sine_wave = matlab_sine_wave(t_axis);
27 else
28     final_sine_wave = A * sin(B * t_axis + C) + D;
29 end
30
31 %% Frequency from x - T sine wave
32 [~, peak_indices] = findpeaks(final_sine_wave, 1);
33 period = diff(t_axis(peak_indices([1, 2])));
34 Frequency = 1/period;
35
36 Amplitude2 = max(final_sine_wave)-min(final_sine_wave);
37
38 end

```

12.2 Fluid Energy Calculations

```

1 function [Fluid_Energy] = Get_Fluid_Energy(Frequency, Ct, U, x)
2
3 pks = findpeaks(x);
4 Disp = mean(pks); % Takes the assumption that flapping at a singular
5 % windspeed is consistent
6 rho = 1.225; % Fluid density
7 period = (1/Frequency)*0.25; % Takes the assumption that 1/4 of the
8 % period is the time taken to reach maximum displacement
9
10 Fluid_Energy = 0.5 * rho * U^3 * abs(Disp) * Ct * period;
11 end

```

12.3 Mass Ratio Plotting and Bending Stiffness Calculations

```

1 %% Prep
2 clc
3 clear
4 close all force

```

```

5
6 %% Loading Data
7 % F1
8 A_1 = load("0.1mm_A.txt");
9 F_1 = load("0.1mm_F.txt");
10
11 % F2
12 A_05 = load("0.05mm_A.txt");
13 F_05 = load("0.05mm_F.txt");
14
15
16 %% Formatting up data
17 % 0.1 mm
18 a = [0,0; F_1(1,1), 0];
19 aa = [0,0; A_1(1,1), 0];
20 F_1_Up = cat(1, a, F_1(1:3, :));
21 A_1_Up = cat(1, aa, A_1(1:3, :));
22
23 % 0.05 mm
24 b = [0,0; F_05(1,1), 0];
25 bb = [0,0; A_05(1,1), 0];
26 F_05_Up = cat(1, b, F_05(1:3, :));
27 A_05_Up = cat(1, bb, A_05(1:3, :));
28
29 %% Formatting Down Data
30 F_1_Down = F_1(4:end, :);
31 A_1_Down = A_1(4:end, :);
32
33 F_05_Down = F_05(3:end, :);
34 A_05_Down = A_05(3:end, :);
35
36 %% Plotting
37
38 figure(1)
39 tiledlayout(2,1, 'TileSpacing','tight')
40 nexttile
41 hold all
42 grid on
43 % Ups first
44 plot(F_1_Up(:,1), F_1_Up(:, 2), 'LineStyle', '-.', 'Marker', '.', ...
45     'MarkerSize', 16, 'Color', 'r')
46 plot(F_1_Down(:,1), F_1_Down(:, 2), 'LineStyle', '--', 'Marker', 'diamond', ...
47     'MarkerSize', 5, 'Color', 'r')

```

```

46 plot(F_05_Up(:,1), F_05_Up(:, 2), 'LineStyle', '-', 'Marker', '.', ' '
      MarkerSize', 16, 'Color', 'b')
47 plot(F_05_Down(:,1), F_05_Down(:, 2), 'LineStyle', '--', 'Marker', ' '
      diamond', 'MarkerSize', 5, 'Color', 'b')
48 legend
49 legend('Location','northwest')
50 legend('$\mu$ = 5.669 Increasing Velocity', '$\mu$ = 5.669 Decreasing
      Velocity', '$\mu$ = 2.835 Increasing Velocity', '$\mu$ = 2.835
      Decreasing Velocity')
51 set(groot,'DefaultTextInterpreter','latex','
      defaultAxesTickLabelInterpreter','latex','defaultLegendInterpreter'
      , 'latex')
52 set(gca,'fontname','times')
53 set(gca,'FontWeight','bold')
54 ylabel('Frequency [Hz]')
55 set(gca, 'XMinorTick', 'on')
56 set(gca, 'YMinorTick', 'on')
57 set(gca,'xticklabel',[])
58 box on
59 title('a) Frequency', 'FontWeight','bold')
60
61 nexttile
62
63 hold all
64 plot(A_1_Up(:,1), A_1_Up(:, 2), 'LineStyle', '-', 'Marker', '.', ' '
      MarkerSize', 16, 'Color', 'r')
65 plot(A_1_Down(:,1), A_1_Down(:, 2), 'LineStyle', '--', 'Marker', ' '
      diamond', 'MarkerSize', 5, 'Color', 'r')
66 plot(A_05_Up(:,1), A_05_Up(:, 2), 'LineStyle', '-', 'Marker', '.', ' '
      MarkerSize', 16, 'Color', 'b')
67 plot(A_05_Down(:,1), A_05_Down(:, 2), 'LineStyle', '--', 'Marker', ' '
      diamond', 'MarkerSize', 5, 'Color', 'b')
68 set(gca, 'XMinorTick', 'on')
69 set(gca, 'YMinorTick', 'on')
70 grid on
71 xlabel('Windspeed [m/s]')
72 ylabel('Amplitude [Deg]')
73 box on
74 set(groot,'DefaultTextInterpreter','latex','
      defaultAxesTickLabelInterpreter','latex','defaultLegendInterpreter'
      , 'latex')
75 set(gca,'fontname','times')
76 set(gca,'FontWeight','bold')

```

```
77 title('b) Amplitude', 'FontWeight','bold')
```

12.4 Taper Ratio Plotting and Bending Stiffness Calculations

```
1 %% Prep
2 clc
3 clear
4 close all force
5
6 %% Loading Data
7 % F1
8 A_2353 = load("2.353_A.txt");
9 F_2353 = load("2.353_F.txt");
10 A2_2353 = load("2.353_A2.txt");
11
12 % F2
13 A_1667 = load("1.667_A.txt");
14 F_1667 = load("1.667_F.txt");
15 A2_1667 = load("1.667_A2.txt");
16
17 % F3
18 A_1 = load("1.0_A.txt");
19 F_1 = load("1.0_F.txt");
20 A2_1 = load("1.0_A2.txt");
21
22 % F4
23 A_078 = load("0.78_A.txt");
24 F_078 = load("0.78_F.txt");
25 A2_078 = load("0.78_A2.txt");
26
27 % F5
28 A_425 = load("0.425_A.txt");
29 F_425 = load("0.425_F.txt");
30 A2_425 = load("0.425_A2.txt");
31
32 %% Formatting up data
33 % 0.78
34 a = [0,0; F_078(1,1), 0];
35 aa = [0,0; A_078(1,1), 0];
36 F_078_Up = cat(1, a, F_078(1:6, :));
37 A_078_Up = cat(1, aa, A_078(1:6, :));
38 A2_078_Up = cat(1, aa, A2_078(1:6, :));
39
```

```

40 % 0.425
41 b = [0,0; F_425(1,1), 0];
42 bb = [0,0; A_425(1,1), 0];
43 F_425_Up = cat(1, b, F_425(1:3, :));
44 A_425_Up = cat(1, bb, A_425(1:3, :));
45 A2_425_Up = cat(1, bb, A2_425(1:3, :));
46
47 % 1.667
48 c = [0,0; F_1667(1,1), 0];
49 cc = [0,0; A_1667(1,1), 0];
50 F_1667_Up = cat(1, c, F_1667(1:7, :));
51 A_1667_Up = cat(1, cc, A_1667(1:7, :));
52 A2_1667_Up = cat(1, cc, A2_1667(1:7, :));
53
54 % 2.353
55 d = [0,0; F_2353(1,1), 0];
56 dd = [0,0; A_2353(1,1), 0];
57 F_2353_Up = cat(1, d, F_2353(1:10, :));
58 A_2353_Up = cat(1, dd, A_2353(1:10, :));
59 A2_2352_Up = cat(1, dd, A2_2353(1:10, :));
60
61 %% Formatting Down Data
62 F_078_Down = F_078(7:end, :);
63 A_078_Down = A_078(7:end, :);
64 A2_078_Down = A2_078(7:end, :);
65
66 F_425_Down = F_425(4:end, :);
67 A_425_Down = A_425(4:end, :);
68 A2_425_Down = A2_425(4:end, :);
69
70 F_1667_Down = F_1667(8:end, :);
71 A_1667_Down = A_1667(8:end, :);
72 A2_1667_Down = A2_1667(8:end, :);
73
74 F_2353_Down = F_2353(11:end, :);
75 A_2353_Down = A_2353(11:end, :);
76 A2_2353_Down = A2_2353(11:end, :);
77
78 F_1_Down = F_1(3:end, :);
79 A_1_Down = A_1(3:end, :);
80 A2_1_Down = A2_1(3:end, :);
81
82

```

```

83 %% Plotting
84
85 figure(1)
86 tiledlayout(2,1, 'TileSpacing','tight')
87 nexttile
88 hold all
89 grid on
90 % Ups first
91 plot(F_2353_Up(:,1), F_2353_Up(:, 2), 'LineStyle', '-','Marker', '.', ...
92      'MarkerSize', 16, 'Color', 'r')
92 plot(F_2353_Down(:,1), F_2353_Down(:, 2), 'LineStyle', '--','Marker', ...
93      'diamond', 'MarkerSize', 5, 'Color', 'r')
93 plot(F_1667_Up(:,1), F_1667_Up(:, 2), 'LineStyle', '-','Marker', '.', ...
94      'MarkerSize', 16, 'Color', 'g')
94 plot(F_1667_Down(:,1), F_1667_Down(:, 2), 'LineStyle', '--','Marker', ...
95      'diamond', 'MarkerSize', 5, 'Color', 'g')
95 plot(F_1_Down(:, 1), F_1_Down(:, 2), 'LineStyle', '--','Marker', ...
96      'diamond', 'MarkerSize', 5, 'Color', "#7E2F8E")
96 plot(F_078_Up(:,1), F_078_Up(:, 2), 'LineStyle', '-','Marker', '.', ...
97      'MarkerSize', 16, 'Color', 'm')
97 plot(F_078_Down(:,1), F_078_Down(:, 2), 'LineStyle', '--','Marker', ...
98      'diamond', 'MarkerSize', 5, 'Color', 'm')
98 plot(F_425_Up(:,1), F_425_Up(:, 2), 'LineStyle', '-','Marker', '.', ...
99      'MarkerSize', 16, 'Color', 'b')
99 plot(F_425_Down(:,1), F_425_Down(:, 2), 'LineStyle', '--','Marker', ...
100     'diamond', 'MarkerSize', 5, 'Color', 'b')
100 legend
101 legend('Location','northwest')
102 legend('F1 Increasing Velocity', 'F1 Decreasing Velocity', 'F2 ...
103     Increasing Velocity', 'F2 Decreasing Velocity',...
103     'F3 Decreasing Velocity', 'F4 Increasing Velocity', 'F4 Decreasing ...
104     Velocity', 'F5 Increasing Velocity', 'F5 Decreasing Velocity')
104 set(groot,'DefaultTextInterpreter','latex',...
105     'defaultAxesTickLabelInterpreter','latex','defaultLegendInterpreter',...
106     'latex')
106 set(gca,'fontname','times')
107 set(gca,'FontWeight','bold')
107 ylabel('Frequency [Hz]')
108 set(gca, 'XMinorTick', 'on')
109 set(gca, 'YMinorTick', 'on')
110 set(gca,'xticklabel',[])
111 box on
112 ylim([0 20])

```

```

113 title('a) Frequency', 'FontWeight','bold')
114
115 nexttile
116
117 % figure(2)
118 hold all
119 plot(A_2353_Up(:,1), A_2353_Up(:, 2), 'LineStyle', '-.', 'Marker', '.', ...
120     'MarkerSize', 16, 'Color', 'r')
120 plot(A_2353_Down(:,1), A_2353_Down(:, 2), 'LineStyle', '--', 'Marker', ...
121     'diamond', 'MarkerSize', 5, 'Color', 'r')
121 plot(A_1667_Up(:,1), A_1667_Up(:, 2), 'LineStyle', '-.', 'Marker', '.', ...
122     'MarkerSize', 16, 'Color', 'g')
122 plot(A_1667_Down(:,1), A_1667_Down(:, 2), 'LineStyle', '--', 'Marker', ...
123     'diamond', 'MarkerSize', 5, 'Color', 'g')
123 plot(A_1_Down(:, 1), A_1_Down(:, 2), 'LineStyle', '--', 'Marker', ...
124     'diamond', 'MarkerSize', 5, 'Color', "#7E2F8E")
124 plot(A_078_Up(:,1), A_078_Up(:, 2), 'LineStyle', '-.', 'Marker', '.', ...
125     'MarkerSize', 16, 'Color', 'm')
125 plot(A_078_Down(:,1), A_078_Down(:, 2), 'LineStyle', '--', 'Marker', ...
126     'diamond', 'MarkerSize', 5, 'Color', 'm')
126 plot(A_425_Up(:,1), A_425_Up(:, 2), 'LineStyle', '-.', 'Marker', '.', ...
127     'MarkerSize', 16, 'Color', 'b')
127 plot(A_425_Down(:,1), A_425_Down(:, 2), 'LineStyle', '--', 'Marker', ...
128     'diamond', 'MarkerSize', 5, 'Color', 'b')
128 set(gca, 'XMinorTick', 'on')
129 set(gca, 'YMinorTick', 'on')
130 grid on
131 xlabel('Windspeed [m/s]')
132 ylabel('Amplitude [${}^{\circ}$]')
133 box on
134 set(groot,'DefaultTextInterpreter','latex',...
135     'defaultAxesTickLabelInterpreter','latex','defaultLegendInterpreter',...
136     'latex')
136 set(gca,'fontname','times')
137 set(gca,'FontWeight','bold')
137 title('b) Amplitude', 'FontWeight','bold')

138
139

140 %% Converting and plotting in dimensionless bending stiffness
141 E = 193e9; % Young's Modulus
142 rho_f = 1.225; % Air density
143 v = 0.25; % Poissons ratio
144 h = 0.1e-3; % Thickness [0.1 mm]

```

```

145
146 L_F1 = 0.0760/(10^-3);
147 L_F2 = 0.0960/(10^-3);
148 L_F3 = 0.1333/(10^-3);
149 L_F4 = 0.1187/(10^-3);
150 L_F5 = 0.0760/(10^-3); % Flag Lengths ^^
151
152 B = (E * h^3)/(12 * (1 - v^2)); % Flexural Rigidity (not dependent on
   flag geometry, only material and thickness
153
154 Beta_F1_Up = B./(rho_f .* F_2353_Up(:,1).^2 * (L_F1*10^(-3))^3);
155 Beta_F2_Up = B./(rho_f .* F_1667_Up(:,1).^2 * (L_F2*10^(-3))^3);
156 Beta_F4_Up = B./(rho_f .* F_078_Up(:,1).^2 * (L_F4*10^(-3))^3);
157 Beta_F5_Up = B./(rho_f .* F_425_Up(:,1).^2 * (L_F5*10^(-3))^3); %
   Bending stiffness increasing velocity ^^
158
159 Beta_F1_Down = B./(rho_f .* F_2353_Down(:,1).^2 * (L_F1*10^(-3))^3);
160 Beta_F2_Down = B./(rho_f .* F_1667_Down(:,1).^2 * (L_F2*10^(-3))^3);
161 Beta_F3_Down = B./(rho_f .* F_1_Down(:,1).^2 * (L_F3*10^(-3))^3);
162 Beta_F4_Down = B./(rho_f .* F_078_Down(:,1).^2 * (L_F4*10^(-3))^3);
163 Beta_F5_Down = B./(rho_f .* F_425_Down(:,1).^2 * (L_F5*10^(-3))^3); %
   Bending stiffness decreasing velocity ^^
164
165 AL_F1_Up = A2_2352_Up(:,2)/L_F1;
166 AL_F2_Up = A2_1667_Up(:,2)/L_F2;
167 AL_F4_Up = A2_078_Up(:,2)/L_F4;
168 AL_F5_Up = A2_425_Up(:,2)/L_F5;
169
170
171 AL_F1_Down = A2_2353_Down(:,2)/L_F1;
172 AL_F2_Down = A2_1667_Down(:,2)/L_F2;
173 AL_F3_Down = A2_1_Down(:,2)/L_F3;
174 AL_F4_Down = A2_078_Down(:,2)/L_F4;
175 AL_F5_Down = A2_425_Down(:,2)/L_F5;
176 AL_F5_Down(8,:) = [];
177
178 figure(2)
179 hold all
180 grid on
181 plot(Beta_F1_Up(:,1), AL_F1_Up(:, 1), 'LineStyle', '-.', 'Marker', '.', %
   'MarkerSize', 16, 'Color', 'r')
182 plot(Beta_F1_Down(:,1), AL_F1_Down(:, 1), 'LineStyle', '--', 'Marker',
   'diamond', 'MarkerSize', 5, 'Color', 'r')

```

```

183 plot(Beta_F2_Up(:,1), AL_F2_Up(:, 1), 'LineStyle', '-', 'Marker', '.', 
      'MarkerSize', 16, 'Color', 'g')
184 plot(Beta_F2_Down(:,1), AL_F2_Down(:, 1), 'LineStyle', '--', 'Marker', 
      'diamond', 'MarkerSize', 5, 'Color', 'g')
185 plot(Beta_F3_Down(:, 1), AL_F3_Down(:, 1), 'LineStyle', '--', 'Marker' 
      , 'diamond', 'MarkerSize', 5, 'Color', "#7E2F8E")
186 plot(Beta_F4_Up(:,1), AL_F4_Up(:, 1), 'LineStyle', '-', 'Marker', '.', 
      'MarkerSize', 16, 'Color', 'm')
187 plot(Beta_F4_Down(:,1), AL_F4_Down(:, 1), 'LineStyle', '--', 'Marker', 
      'diamond', 'MarkerSize', 5, 'Color', 'm')
188 plot(Beta_F5_Up(:,1), AL_F5_Up(:, 1), 'LineStyle', '-', 'Marker', '.', 
      'MarkerSize', 16, 'Color', 'b')
189 plot(Beta_F5_Down(:,1), AL_F5_Down(:, 1), 'LineStyle', '--', 'Marker', 
      'diamond', 'MarkerSize', 5, 'Color', 'b')
190 legend
191 legend('Location','southeast')
192 legend('F1 Increasing Velocity', 'F1 Decreasing Velocity', 'F2 
    Increasing Velocity', 'F2 Decreasing Velocity',...
    'F3 Decreasing Velocity', 'F4 Increasing Velocity', 'F4 Decreasing 
    Velocity', 'F5 Increasing Velocity', 'F5 Decreasing Velocity')
193 set(groot,'DefaultTextInterpreter','latex','
    defaultAxesTickLabelInterpreter','latex','defaultLegendInterpreter'
    , 'latex')
194 set(gca,'fontname','times')
195 set(gca,'FontWeight','bold')
196 ylabel('A/L')
197 xlabel('$\beta$')
198 set(gca, 'XMinorTick', 'on')
199 set(gca, 'YMinorTick', 'on')
200 box on
201 title('A/L vs $\beta$', 'FontWeight','bold')

```

12.5 Example Processing Script: $\lambda = 2.353$

```

1 %% Prep
2 clc
3 clear
4 close all force
5
6 %% Data Import
7 header = 2;
8 delimiter = '\t';
9 CT_1 = 0.08;

```

```
10 Frequency(:,1) = [10.03
11 10.77
12 11.80
13 13.04
14 13.90
15 14.72
16 16.22
17 17.59
18 18.02
19 18.45
20 17.14
21 16.22
22 14.18
23 12.44
24 11.47
25 10.41
26 9.63
27 8.79];
28
29 Amplitude(:,1) = [10.03
30 10.77
31 11.80
32 13.04
33 13.90
34 14.72
35 16.22
36 17.59
37 18.02
38 18.45
39 17.14
40 16.22
41 14.18
42 12.44
43 11.47
44 10.41
45 9.63
46 8.79];
47
48 for i = 2380:1:2387
49     filename = [num2str(i), '.txt'];
50     dat = importdata(filename, delimiter, header);
51     Data = dat.data;
52
```

```

53 Time = Data(:,1);
54 x = Data(:,2);
55 y = Data(:,3);
56
57 [Frequency(i - 2379,2), Amplitude(i - 2379,2), Amplitude2(i -
58 2379,2)] = get_Freq_Amp(Time, x, y, [], [], [], []);
59
60 end
61
62 for i = 2388
63 filename = [num2str(i), '.txt'];
64 dat = importdata(filename, delimiter, header);
65 Data = dat.data;
66
67 Time = Data(:,1);
68 x = Data(:,2);
69 y = Data(:,3);
70
71 [Frequency(i - 2379,2), Amplitude(i - 2379,2), Amplitude2(i -
72 2379,2)] = get_Freq_Amp(Time, x, y, 2.4e1, 5.56e1, -1.29e2, 4.2
73 e1);
74 [Fluid_Energy_2353(i-2379,1)] = Get_Fluid_Energy(Frequency(i
75 -2379,2), CT_1, Frequency(i-2379,1), x*10^(-3));
76 end
77 for i = 2389
78 filename = [num2str(i), '.txt'];
79 dat = importdata(filename, delimiter, header);
80 Data = dat.data;
81
82 Time = Data(:,1);
83 x = Data(:,2);
84 y = Data(:,3);
85
86 [Frequency(i - 2379,2), Amplitude(i - 2379,2), Amplitude2(i -
87 2379,2)] = get_Freq_Amp(Time, x, y, 1.14e1, 6.7e1, -6.29e1,
5.99e1);
88 [Fluid_Energy_2353(i-2379,1)] = Get_Fluid_Energy(Frequency(i
-2379,2), CT_1, Frequency(i-2379,1), x*10^(-3));
89 end
90 for i = 2390:1:2397

```

```

88 filename = [num2str(i), '.txt'];
89 dat = importdata(filename, delimiter, header);
90 Data = dat.data;
91
92 Time = Data(:,1);
93 x = Data(:,2);
94 y = Data(:,3);
95
96 [Frequency(i - 2379,2), Amplitude(i - 2379,2), Amplitude2(i -
97 2379,2)] = get_Freq_Amp(Time, x, y, [], [], [] ,[]);
98 [Fluid_Energy_2353(i-2379,1)] = Get_Fluid_Energy(Frequency(i
99 -2379,2), CT_1, Frequency(i-2379,1), x*10^(-3));
100 end
101
102 save("2.353_F.txt", "Frequency", "-ascii")
103 save("2.353_A.txt", "Amplitude", "-ascii")
104 save("2.353_A2.txt", "Amplitude2", "-ascii")
105 save("2.353_FE.txt", "Fluid_Energy_2353", "-ascii")

```

13 Appendix C: Example Data Sets for $\lambda = 2.353$

13.1 12.44 ms^{-1} Raw Data

Table 6: 12.44 ms^{-1} raw data output from Physlets Tracker software

Time [s]	X Displacement [mm]	Y Displacement [mm]
0.000	66.35	0.594
0.017	59.71	40.48
0.033	11.32	75.75
0.050	-64.39	32.73
0.067	-67.53	10.75
0.083	-52.57	52.48
0.100	4.492	77.41
0.117	68.57	6.504
0.133	67.83	20.35
0.150	38.84	63.19
0.167	-31.33	69.66
0.184	-66.42	4.103
0.200	-64.39	31.06
0.217	-29.49	69.84
0.234	53.43	51.19

Continued on next page

Table 6 – continued from previous page

Time [s]	X Displacement [mm]	Y Displacement [mm]
0.250	65.80	2.256
0.267	57.12	42.51
0.284	8.001	75.75
0.300	-65.49	29.59
0.317	-67.89	10.94
0.334	-50.91	54.33
0.350	10.40	76.67
0.367	66.91	2.441
0.384	65.62	22.94
0.400	37.55	66.89
0.417	-39.46	65.04
0.434	-66.79	2.441
0.450	-63.28	34.94
0.467	-25.05	72.43
0.484	59.15	44.36
0.501	66.54	5.026
0.517	56.01	46.76
0.534	1.907	77.04
0.551	-66.23	24.05
0.567	-68.63	14.07
0.584	-48.87	57.29
0.601	14.09	74.83
0.617	67.28	1.148
0.634	64.69	26.08
0.651	34.96	68.92
0.667	-43.89	60.61
0.684	-66.23	2.995
0.701	-61.80	36.79
0.717	-21.36	73.90
0.734	63.03	36.05
0.751	65.98	6.319
0.767	53.98	49.90
0.784	-4.371	76.31
0.801	-66.60	14.44
0.817	-66.79	17.58
0.834	-45.55	60.61
0.851	23.70	72.24
0.868	65.43	0.594
Continued on next page		

Table 6 – continued from previous page

Time [s]	X Displacement [mm]	Y Displacement [mm]
0.884	65.62	29.40
0.901	31.08	70.21
0.918	-48.87	55.62
0.934	-67.34	5.396
0.951	-61.43	40.11
0.968	-16.37	74.83
0.984	64.51	31.99
1.001	64.51	8.350
1.018	53.80	51.75
1.034	-6.957	76.12
1.051	-68.45	12.04
1.068	-66.60	19.06
1.084	-46.29	63.01
1.101	25.36	71.32
1.118	66.72	-0.883
1.134	64.69	30.14
1.151	29.42	72.43
1.168	-51.46	52.85
1.185	-67.16	4.842
1.201	-59.22	42.70
1.218	-11.94	76.31
1.235	66.17	24.05
1.251	66.17	10.94
1.268	51.21	53.59
1.285	-12.13	75.75
1.301	-67.53	12.23
1.318	-67.34	20.17
1.335	-42.97	62.27
1.351	25.54	72.80
1.368	67.46	1.702
1.385	63.95	29.77
1.401	29.98	71.32
1.418	-47.03	58.39
1.435	-66.97	5.211
1.451	-62.17	40.11
1.468	-18.77	74.27
1.485	62.66	36.97
1.502	67.09	6.504
Continued on next page		

Table 6 – continued from previous page

Time [s]	X Displacement [mm]	Y Displacement [mm]
1.518	54.72	50.08
1.535	-3.817	76.86
1.552	-67.16	17.40
1.568	-67.71	16.66
1.585	-47.03	58.76
1.602	20.19	74.27
1.618	65.25	1.887
1.635	65.25	27.74
1.652	31.45	69.10
1.668	-48.87	56.36
1.685	-66.79	3.918
1.702	-60.88	40.11
1.718	-15.64	75.94
1.735	65.43	29.40
1.752	67.28	7.981
1.768	51.95	52.11
1.785	-8.988	76.12
1.802	-67.89	13.71
1.818	-67.89	18.69
1.835	-43.15	62.09
1.852	24.81	71.32
1.869	66.17	1.887
1.885	64.51	29.77
1.902	29.79	70.40
1.919	-48.51	56.55
1.935	-67.53	5.396
1.952	-61.25	40.30
1.969	-16.56	75.01
1.985	65.06	31.25
2.002	66.35	7.796
2.019	52.69	51.75
2.035	-8.988	77.04
2.052	-67.16	12.41
2.069	-66.79	19.80
2.085	-42.60	61.90
2.102	26.28	73.17
2.119	65.43	1.148
2.135	63.95	31.06

Continued on next page

Table 6 – continued from previous page

Time [s]	X Displacement [mm]	Y Displacement [mm]
2.152	26.28	72.06
2.169	-49.98	53.59
2.186	-66.60	6.688
2.202	-60.88	40.85
2.219	-15.64	75.20
2.236	63.03	34.02
2.252	65.25	9.089
2.269	52.32	50.45
2.286	-5.479	76.49
2.302	-67.16	17.58
2.319	-66.79	17.58
2.336	-46.47	59.69
2.352	20.74	72.98
2.369	65.80	2.072
2.386	64.14	28.29
2.402	30.34	69.47
2.419	-48.32	55.99
2.436	-66.23	4.288
2.452	-60.51	39.19
2.469	-15.27	75.01
2.486	64.32	28.85
2.503	66.35	9.089
2.519	51.21	52.48
2.536	-11.20	75.75
2.553	-67.89	10.94
2.569	-66.23	20.35
2.586	-42.60	62.83
2.603	30.53	69.84
2.619	65.06	-0.514
2.636	63.21	31.25
2.653	25.73	72.06
2.669	-53.49	51.75
2.686	-67.34	5.026
2.703	-59.03	43.07
2.719	-10.47	76.31
2.736	66.54	20.72
2.753	69.12	11.86
2.769	48.81	56.36
Continued on next page		

Table 6 – continued from previous page

Time [s]	X Displacement [mm]	Y Displacement [mm]
2.786	-13.05	75.75
2.803	-68.26	11.12
2.819	-66.23	21.09
2.836	-41.86	63.01
2.853	29.42	70.95
2.870	66.17	0.410
2.886	64.51	30.32
2.903	26.84	72.06
2.920	-53.31	51.93
2.936	-67.71	4.657
2.953	-60.14	43.25
2.970	-10.10	75.94
2.986	65.98	22.20
3.003	67.46	11.49
3.020	49.73	55.81
3.036	-15.08	75.01
3.053	-66.79	7.058
3.070	-66.05	22.38
3.086	-38.35	65.23
3.103	40.69	64.49
3.120	64.14	-0.144
3.136	61.00	35.86
3.153	18.16	73.90
3.170	-62.54	38.45
3.187	-67.53	7.058
3.203	-56.45	48.61
3.220	6.059E-2	77.41
3.237	66.17	8.719
3.253	66.72	16.48
3.270	41.79	62.64
3.287	-27.64	70.95
3.303	-66.23	2.626
3.320	-65.31	29.77
3.337	-29.85	70.21
3.353	52.87	52.30
3.370	65.80	2.072
3.387	57.12	43.81
3.403	7.078	75.38

13.2 Processing script output data

Table 7: Wind speed, angular amplitude, frequency and fluid energy calculated outputs

Wind speed [ms ⁻¹]	Amplitude [°]	Frequency [Hz]	Fluid Energy [J]
10.03	125.5401	8.5629	9.3046913e-02
10.77	145.4683	8.5632	1.1969261e-01
11.80	155.8071	8.5624	1.5912684e-01
13.04	174.3057	8.5629	2.1044771e-01
13.90	183.5464	8.5626	2.5301027e-01
14.72	189.8294	7.4936	3.5020578e-01
16.22	203.5415	6.6600	5.2249258e-01
17.59	214.4178	5.4499	3.7626598e-01
18.02	211.5588	8.5630	4.4375065e-01
18.45	156.9373	9.9900	5.2857409e-01
17.14	208.3634	5.9946	4.1840135e-01
16.22	205.9111	6.6603	4.7635523e-01
14.18	186.2899	7.4932	3.0984145e-01
12.44	168.8970	8.5639	1.8266649e-01
11.47	154.2276	8.5622	1.4211115e-01
10.41	135.6112	8.5618	1.0699337e-01
9.63	124.8256	8.5624	8.2021614e-02
8.79	107.7783	8.5625	5.6789057e-02